King's Research Portal

DOI:
10.1016/j.rse.2017.12.016

Document Version
Peer reviewed version

Link to publication record in King's Research Portal

Citation for published version (APA):
Mota, B., & Wooster, M. J. (2018). A New Top-Down Approach for Directly Estimating Biomass Burning Emissions and Fuel Consumption Rates and Totals from Geostationary Satellite Fire Radiative Power (FRP). *REMOTE SENSING OF ENVIRONMENT*, *206*, 45-62. https://doi.org/10.1016/j.rse.2017.12.016

Citing this paper
Please note that where the full-text provided on King's Research Portal is the Author Accepted Manuscript or Post-Print version this may differ from the final Published version. If citing, it is advised that you check and use the publisher's definitive version for pagination, volume/issue, and date of publication details. And where the final published version is provided on the Research Portal, if citing you are again advised to check the publisher's website for any subsequent corrections.

General rights
Copyright and moral rights for the publications made accessible in the Research Portal are retained by the authors and/or other copyright owners and it is a condition of accessing publications that users recognize and abide by the legal requirements associated with these rights.

- Users may download and print one copy of any publication from the Research Portal for the purpose of private study or research.
- You may not further distribute the material or use it for any profit-making activity or commercial gain
- You may freely distribute the URL identifying the publication in the Research Portal

Take down policy
If you believe that this document breaches copyright please contact librarypure@kcl.ac.uk providing details, and we will remove access to the work immediately and investigate your claim.

Download date: 29. Dec. 2024

A New Top-Down Approach for Directly Estimating Biomass Burning Emissions and Fuel Consumption Rates and Totals from Geostationary Satellite Fire Radiative Power (FRP)

Authors:

Bernardo Mota[1,2] and Martin J. Wooster[1,3,*]

[1] King's College London, Department of Geography, Strand, London WC2R 2LS, UK.

[2] Present address: European Commission, Joint Research Centre, Ispra, Italy.

[3] NERC National Centre for Earth Observation (NCEO), King's College London, Strand, London WC2R 2LS, UK.

*corresponding author (martin.wooster@kcl.ac.uk)

Keywords: Fire Emissions, FRP, FRE, Geostationary, southern Africa, Meteosat SEVIRI

Abstract

Regional to global-scale biomass burning emissions inventories are primarily based on satellite-derived burned area or fire radiative power (FRP), and most rely on conversions to fuel consumption prior to the emissions estimation stage. This is generally considered the step introducing greatest uncertainty, and some apparently discrete inventories are not fully independent, as they have been cross-calibrated to aid this stage. We present a novel emissions inventory approach that bypasses the fuel consumption step, directly linking geostationary FRP measures to emission rates of total particulate matter (TPM), via coefficients derived from observations of smoke plume aerosol optical depth (AOD). The approach is fully 'top-down', being based on spaceborne observations alone, is performed at or close to the FRP data's original pixel resolution, and avoids the need to assume or model fuel consumption per unit area prior to the emissions calculation. Rates and totals of trace gas and carbon emission can be inferred from the TPM fluxes, and in combination with satellite burned area (BA) products the approach provides an innovative top down approach to mapping fuel consumption per unit area (kg.m^{-2}) as a last step in the calculation. Using this innovative methodology, which we term 'FRE$_{\text{emissions}}$' (FREM), we generate a 2004 – 2012 fire emissions inventory for southern Africa, based on Meteosat FRP-PIXEL data. We find basic annual average TPM emissions 45% higher than the widely used GFASv1.2 inventory, with our higher totals in line with independent assessments that necessitate a significant upscaling of GFAS TPM emissions to match observed AODs. Our estimates are also 12% higher than GFEDv4.1s, which already includes a substantial upward adjustment for fires too small to be detected by the MODIS MCD64A1 BA product. If we adjust the FREM-derived emissions for SEVIRI's inability to detect the lower FRP component of the regions fire regime then the differences between FREM and GFAS / GFED grow further, to a mean of 64% with respect to GFED4.1s TPM emissions for example. These upwardly adjusted FREM estimates

agree very well with FEER, an FRP- and AOD-based inventory driven by polar-orbiting MODIS FRP ‘snapshots’ rather than geostationary observations. Similarly higher totals are seen for FREM’s fire-emitted trace gases, derived using the emission factor ratios of gases to particulates. Our exploitation of geostationary FRP requires fewer assumptions than use of polar orbiter FRP measures, avoids biases coming from incomplete sampling of the fire diurnal cycle, and enables the FREM approach to provide fire emissions and fuel consumption estimates at a higher spatio-temporal resolution than any inventory currently available (e.g. 0.05°, and hourly averages or better), including per km^2 of area burned. The approach offers great potential to generate very high resolution fire emissions datasets for the tropics, sub-tropics and potentially temperate zones, with updates available in near real-time from the global suite of geostationary meteorological satellites operated by organisations such as EUMETSAT (Meteosat), NOAA (GOES) and JMA (Himawari).

1. INTRODUCTION

Accurate inventories of landscape fire emissions are required to assess influences on regional and global atmospheric composition, weather and climate (Andreae and Merlet, 2001; Akagi *et al.*, 2011). Biomass burning is amongst the greatest source of atmospheric fine particulate matter ($PM_{2.5}$ and PM_{10}; Reddington *et al.,* 2016), resulting in significant impacts on human health (Pope *et al.* 2002). For certain air pollutants like carbon monoxide (CO), landscape fires are among the most dominant source (Andreae and Merlet, 2001), whilst for others (e.g. hydrogen cyanide; HCN) seemingly the only major source (Li *et al.*, 2000). Every landscape fire emits CO_2 as its main product (Andreae and Merlet, 2001; Wooster *et al.*, 2011), even those dominated by smouldering combustion (e.g. Huijnen *et al.*, 2016), and fires in tropical forests and peatlands contribute very significantly to the net growth of atmospheric CO_2 (van der Werf *et al.*, 2009; Huijnen *et al.*, 2016).

Landscape fire emissions show large variabilities across all timescales (e.g. Roberts and Wooster, 2008; Roberts *et al.*, 2009; van der Werf *et al.,* 2011; Kaiser *et al.,* 2012; Andela *et al.*, 2016), and only satellite Earth Observation (EO) can drive large-scale, regularly updated emissions inventories. Thus far, no inventory delivers both relatively fine (e.g. ~ hourly or better) spatial and temporal (e.g. ~ 5 km or better) resolution, nor full agreement with independent atmospheric observations (e.g. see comparisons by Shi *et al.*, 2015; Pereira *et al.*, 2016; Reddington *et al.,* 2016). Differences stem from (i) limitations in the EO data and algorithms used for fire identification and characterisation (e.g. Boschetti *et al.*, 2004; Freeborn *et al.*, 2009; Randerson *et al.*, 2012; Nogueira *et al.*, 2016), (ii) difficulties in estimating fuel consumption per unit area ($kg.m^{2)}$ and total fuel consumption (kg) for the identified fires (e.g. Reid *et al.*, 2009; Roberts *et al.*, 2011; Kaiser *et al.*, 2012), and (iii) uncertainties involved in estimating emissions of particulates and gases from fuel consumption totals (e.g. Vermote *et al.*, 2009; Van Leeuwen *et* *al.*, 2011). Whilst EO data and algorithms for use in (i) have improved substantially based on polar orbiting MODIS and VIIRS (e.g. Boschetti *et al.*, 2004; Giglio *et al.*, 2013; 2016; Schroeder *et al.*, 2014), and second generation geostationary systems such as Meteosat SEVIRI (e.g. Wooster *et al.,* 2005; 2015), and more detailed emissions factor databases have become available for use in (iii) (e.g. Akagi *et al.*, 2011; Huijnen *et al.*, 2016), there has been relatively less progress in (ii) with regards to converting satellite fire radiative power (MW) or burned area (m^2) measures into fuel consumption estimates (Andela *et al.*, 2016). This remains an area of key uncertainty (Reid *et al.*, 2009), and for this reason we focus here on a new fire emissions methodology that bypasses the fuel consumption estimation step and directly relates fire emissions to FRP observations, the latter available at very high temporal resolution from geostationary orbit. This innovative approach significantly limits the number of assumptions required in the emissions calculation, particularly compared to burned area based methods, and reduces sources of uncertainty involved in the 'fuel consumption estimation' stage that pose difficulties even when combining burned area and FRP data together (e.g. Roberts *et al.*, 2011; Andela *et al.*, 2016). Our approach builds on research with polar orbiting satellite FRP and AOD data started by Ichoku and Kaufman (2005), but by using the near continuous geostationary FRP observations we limit the assumptions required. We term this new methodology '$\mathrm{FRE}_{\mathrm{emissions}}$' (FREM), since use of temporally-integrated geostationary FRE data are key. Fuel consumption (kg), including on a per unit area basis ($kg.m^{-2}$), can be estimated as a last step if required, based on either the inverse of the TPM emissions factor or the calculated total carbon in the emissions released.

2. LANDSCAPE FIRES AND EMISSIONS INVENTORY METHODOLOGIES

Landscape fires occur in most vegetated ecosystems. Most herbaceous biomes typically show finer fuels and more flaming combustion, along with lower fuel consumptions per unit area [$kg.m^{-2}$] and the strongest dominance of CO_2 in their smoke (Akagi *et al.*, 2011; Wooster *et al.*, 2011; van Leeuwen *et al.*, 2014). Fires in more wooded areas, along with those burning organic soils such as peat, typically show higher fuel consumptions per unit area, a tendency towards more smouldering combustion, and higher proportions of CO and total particulate matter (TPM) in their smoke (e.g. Andreae and Merlet, 2001; Huijnen *et al.*, 2016). All current emissions inventories use emission factors [EF_x, g.kg^{-1}]) to specify how much of chemical species x is released per kg of fuel consumed. The biome-dependent summary EFs of Andreae and Merlet (2001) and its updates (e.g. as reported in Kaiser *et al.*, 2012), and/or those in Akagi *et al.* (2011), are used in most cases. Therefore, the primary reason independent fire emissions inventories show not only spatial and temporal discrepancies, but also differences in magnitude, comes not from the deployed EFs but from the differing estimates of total fuel consumption (e.g. Roberts *et al.*, 2011; Larkin *et al.*, 2014 Knorr *et al.*, 2012; Kaiser *et al.*, 2012). This is in part because fuel consumptions per unit area vary markedly, even within the same biome (e.g. Reid *et al.*, 2009; Kukavskaya *et al.*, 2012; Sommers *et al.*, 2014; van Leeuwen *et al.*, 2014; Weise and Wright, 2014; Andela *et al.*, 2016), and this variability is difficult to track precisely.

2.1 Burned Area Based Methodologies

Most 'bottom up' approaches to fire emissions estimation are currently driven by burned area (BA) measures [m^2], mostly derived from daily 500 m spatial resolution MODIS data (e.g. Giglio *et al.*, 2013). This highly successful approach delivers high quality BA mapping across many biomes, though smaller burns can remain undetected and lead to significant fire emissions underestimation in 'small-fire' dominated ecosystems (Randerson *et al.*, 2012; Zhang et al., 2017). To estimate total fuel consumption, the BA data must be combined with fuel consumption per unit area [kg.m^{-2}] estimates, themselves calculated from somewhat uncertain fuel load [FL; kg.m^{-2}] and 'combustion completeness' [C; unitless] metrics (Reid *et al.*, 2009; Vermote *et al.*, 2009; van Leeuwen *et al.,* 2014). Successful emissions inventories such as the widely used Global Fire Emissions Database (GFED; van der Werf *et al.*, 2010) use this bottom-up formulation to deliver spatially explicit fuel consumption totals to which biome specific EFs are then applied, and GFED currently delivers monthly emissions estimates (0.25° grid cells) around a year after the MODIS MCD64A1 BA data become available. To account for unmapped 'small fire' BA, the most recent GFED v4.1s also applies a BA 'boost' based on active fire detections (Van der Werf *et al.*, 2017), though the methodology (based on Randerson *et al.,* 2012) remains to be fully validated.

2.2 FRP Based Methodologies

An alternative to BA-based fire emissions inventory methods are FRP-based approaches, where FRP observations integrated over a fire's lifetime are used to estimate fire radiative energy (FRE) release. Since even fires covering 10^{-3} to 10^{-4} of a pixels area can be detected from polar or geostationary orbit, even rather small fires can be included in this integration (Roberts *et al.*, 2005). However, some fires will remain below the sensors minimum FRP detection limit (Roberts et al., 2015). Furthermore, whilst small-scale experiments show FRE is directly relatable to total fuel consumption with minimal dependence on vegetation type (Wooster *et al.* 2002; 2005; Kremens *et al.*, 2012), the linear scalar between FRE and biomass burned may show a biome dependence when observing FRP from orbit, in part because different proportions of the fire-emitted FRP maybe missed across different biomes (e.g. because of variable tree canopy cover; Freeborn *et al.,* 2009). Nevertheless, FRP approaches can in theory (i) remove reliance on the more difficult-to-estimate fuel load and combustion completeness metrics required by 'bottom up' methods, (ii) enable impacts of far smaller fires to be incorporated than when using burned area measures alone (Wooster *et al.,* 2005; Kaiser *et al.*, 2012), and (iii) provide much quicker information delivery, at higher temporal resolutions, than BA-based methods (e.g. Kaiser *et al.*, 2012; Hertwig *et al.*, 2013; Roberts *et al.*, 2015; Huijnen *et al.*, 2016). However, the simple and consistent conversion between FRP and fuel consumption rate found in the laboratory (e.g. Wooster *et al.*, 2005) may not hold between biomes when using satellite FRP measures, and if only polar orbiting FRP ‘snapshots’ are used then most burning occurs when fires are not being observed by the sensor.

The most widely used FRP-based emissions inventory is delivered by the Global Fire Assimilation System (GFAS: Kaiser *et al.*, 2012), operated as part of the Copernicus Atmosphere Monitoring Service (CAMS: https://atmosphere.copernicus.eu/). GFAS uses the FRP approach to map mean fuel consumption globally (daily, 0.1°) from weighted averages of MODIS’ FRP ‘snapshots’. GFAS’ conversion between FRP and fuel consumption is based on biome-specific conversion factors [β, kg.MJ^{-1}] derived from comparisons between GFAS’ monthly FRP totals and the matching GFED v3.1 dry matter fuel consumptions (Kaiser *et al.*, 2012). This is a pragmatic and sensible solution to converting satellite-derived FRP data into fuel consumption estimates, but has the disadvantage of building back into the FRP-based approach uncertainties inherent in GFEDs pre-fire fuel load and combustion completeness parameters (Reid *et al.*, 2009; Vermote *et al.*, 2009), as well as any biome-dependent biases in the MODIS BA product (e.g. Giglio *et al.*, 2013). It also means that GFAS and GFED are driven to provide rather similar fuel consumption totals and thus fire emissions, limiting their independence (Kaiser *et al.*, 2012). More independent FRP-based methodologies are provided by the Fire Energetic and Emissions Research (FEER) system (Ichoku and Ellison, 2014), the Brazilian Biomass Burning Emission Model with FRP assimilation (3BEM_FRP) (Pereira *et al.*, 2016) and IS4FIRES (Soares *et al.*, 2015), which all relate MODIS FRP measures directly to fire emissions without recourse to a fuel consumption estimation stage. Our new FREM methodology builds on this type of formulation - extending it to exploit the advantages of geostationary FRP observations in order to avoid the many spatio-temporal sampling issues inherent in use of polar-orbiting FRP data alone (which can lead to FRE under- or over-estimation (Roberts *et al.*, 2009; Freeborn *et al.*, 2011; Wiedinmyer *et al.*, 2011; Kaiser *et al.*, 2012; Andela *et al.*, 2015). Use of multi-day MODIS FRP data can reduce such sampling biases, but creates only low temporal resolution FRE estimates (Vermote *et al.*, 2009; Freeborn *et al.*, 2011). Combining FRP snapshots with diurnal cycle parameterisations may provide higher frequency estimates, assuming the early afternoon MODIS overpass roughly captures the daily fire activity peak (e.g. Ellicott *et al.*, 2009; Vermote *et al.*, 2009; Freeborn *et al.*, 2011; Andela *et al.* 2015), but as demonstrated in Fig. 1 the time difference between the maxima of the fire diurnal cycle and the afternoon MODIS overpass shows significant spatial variation, as does the fraction of the total daily fire pixel count that occurs during the MODIS overpass window (Fig. 2). Where the latter is particularly low, daily FRE (or average FRP) measures derived from MODIS are more prone to bias, potentially leading to spatially varying differences between such FRE totals and actual fuel consumptions. This is likely to be a key driver of the need for GFAS' biome-dependent conversion factors [β] that link daily MODIS-derived FRE and fuel consumption (Kaiser *et al.,* 2012), with additional factors including biome dependent biases in the MCD64A1 BA data that drive GFED, to which GFAS is calibrated (Giglio *et al.*, 2013).

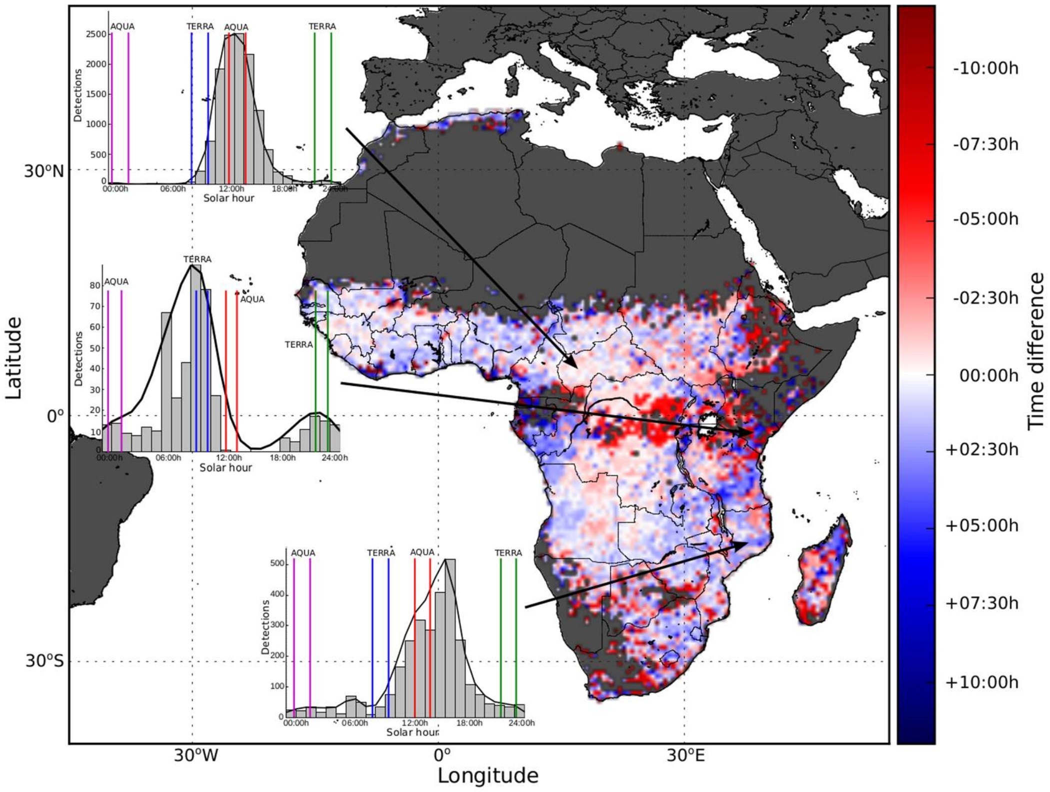

Figure 1. Mapped difference (hrs) between the time of maximum active fire pixel count (i.e. daily fire activity peak) and the ± 1 hr window encompassing the MODIS local solar overpass time (which depends on changing location within the MODIS swath). Data are for 2010 and based on Meteosat Second Generation (MSG) SEVIRI FRP-PIXEL Product available from the EUMETSAT LSA SAF (Wooster *et al.*, 2015), spatially aggregated into 0.5° grid cells. Subset graphs show example histograms of FRP-PIXEL active fire detections for three 0.5° grid cells located over eastern Central African Republic, Northern Mozambique, and southern Kenya, with a functional fit to these data and the four MODIS overpass windows per day also indicated. Only fire detections with confidences > 50% are included (Wooster *et al.,* 2015).

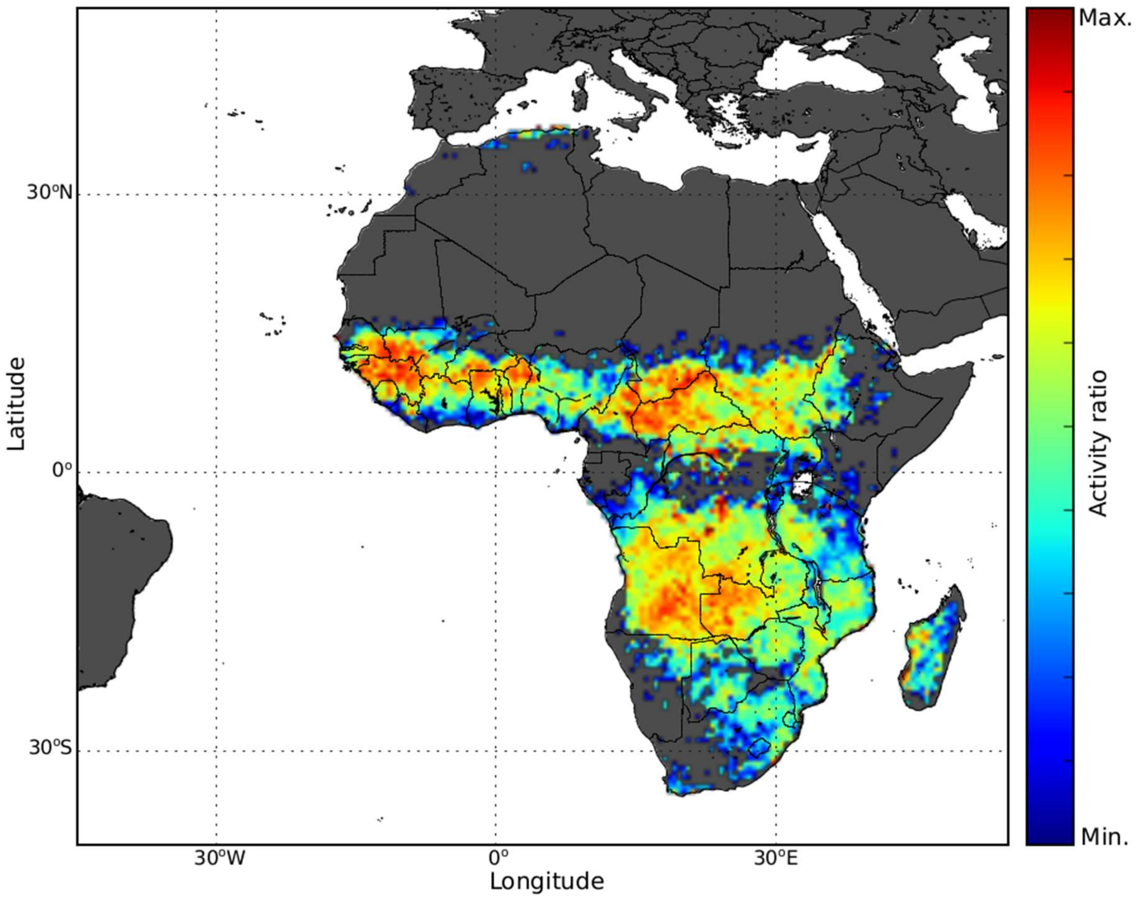

Figure 2. Spatial distribution of active fire detection opportunities offered by the MODIS sampling windows shown in Fig. 1. This is expressed as the ratio of the Meteosat SEVIRI FRP-PIXEL active fire detections made within the ± 1 hr window surrounding the four daily MODIS overpass times (shown in Fig. 1) to the total number of daily detections. Source data are those of Fig. 1.

Further factors challenging the use of spatially-invariant FRE to fuel consumption conversion factors, is that spaceborne FRP data are subject to geographically-varying measurement artefacts absent from laboratory-scale observations. These include (i) blocking of a proportion of surface fire FRP by any overlying tree canopy (e.g. Freeborn *et al.,* 2014; Mathews *et al.*, 2016), (ii) FRE-biases caused by the presence of different proportions of active fire pixels below the sensors FRP detection limit (e.g. Schroeder *et al.*, 2008; Freeborn *et al.*, 2009; Roberts *et al.*, 2015), and (iii) varying flame depths and soot volume fractions leading to varying flame emissivity's (Johnson *et al.*, 2015). The magnitude of such artefacts depends on the ecosystems vegetation and/or fire regime (Edwards, 1984; Chuvieco *et al.*, 2008), furthering the biome dependence of satellite-derived FRP (or FRE) to fuel consumption relations.

3. DETAIL ON THE FRE$_{\text{EMISSIONS}}$ APPROACH TO FIRE EMISSIONS ESTIMATION

FREM is designed to deal with a series of limitations that currently impact use of the satellite fire radiative power approach by;

(i) Removing observation biases that stem from the incomplete sampling of the fire diurnal cycle provided by polar-orbiters. FREM uses geostationary FRP observations, and in addition to removing the type of biases shown in Fig. 1, further benefits of such near-continuous FRP data in relation to smoke emissions transport modelling have been demonstrated by e.g. Baldassarre *et al.* (2015) and Roberts *et al.*, (2015).

(ii) Deriving relations that link FRP to fire emissions fluxes and fuel consumption rates that inherently account for gross, inter-biome variations in FRP measurement bias. Such biases include, the changing wavelength-dependent emissivity of flames that will vary between fire types dominating the different biomes (Johnson *et al.*, 2015), and the changing degree of tree-canopy interception of surface fire FRP, highlighted as an issue by Freeborn *et al.* (2014) and demonstrated by Matthews *et al.* (2016).

(iii) Removing the need to link satellite FRP observations to fuel consumption rates using factors derived in small scale experiments that may not be fully representative when using satellite-FRP measures of landscape scale fires (e.g. Wooster *et al.*, 2005), or which are based on landscape-scale fuel consumption metrics stemming from burned-area based emissions inventories such as GFED. Use of the latter by e.g. Kaiser *et al.* (2012) removes the independence of the FRP-based emissions calculations and builds into the methodology issues affecting BA based inventories, such as current inabilities to detect many 'small area' and/or sub-canopy fires (Randerson *et al.* 2012) and uncertainties in the fuel load per unit area and 'combustion completeness' terms (Reid *et al.*, 2009).

FREM estimates emissions of total particulate matter (TPM) directly from geostationary FRP data via application of biome-dependent ′smoke emissions coefficients′ [C_{biome},], these being calculated from per-fire matchups of FRE and smoke plume aerosol optical depth (AOD). Freeborn *et al.* (2008) and Ichoku *et al.* (2008) already demonstrated strong relations between FRP and aerosol flux in the laboratory, and applying this approach to satellite derived FRP data removes many of the assumptions and interdependences discussed in Section 2. Trace gas fluxes can be subsequently estimated from the TPM emissions via application of the appropriate emissions factor ratios.

The FEER approach of Ichoku and Ellison (2014) already uses biome-dependent TPM 'smoke' emissions coefficients [C_{biome}, [kg.MW^{-1}]) to deliver a ′top down′ emissions methodology fully independent of fuel consumption-based methods. FEERs coefficients were derived from combinations of instantaneous MODIS FRP (MW or J.s^{-1}) and TPM emission rate (F_e, [kg.s^{-1}])

data, the latter calculated from simultaneously timed MODIS AOD products combined with plume height and wind-speed estimates. Smoke plume heights are often rather uncertain (e.g. Sofiev *et al.*, 2012; Paugam *et al.*, 2016), and a single FRP measure may not reflect the time-integrated FRP characteristics a fire typically shows over the hours needed to generate the type of large-scale plume observable in the 10 km MODIS AOD data (Baldassarre *et al.*, 2015; Roberts *et al.*, 2015). Indeed, bias seems likely because some of the smoke present in these large plumes will have been generated earlier in the diurnal cycle than the MODIS FRP observation made simultaneously with the AOD assessment. To help counteract this, Ichoku and Ellison (2014) match only part of the plume to the instantaneous FRP measure, which required assumptions on wind speed and direction at plume height. A key advantage of FREM's use of semi-continuous geostationary FRP data is that it allows each matchup to be based on the fire's entire FRP time-series, and its entire smoke plume AOD recorded at the moment of the MODIS overpass, removing the sampling-time bias, reliance on smoke plume height and velocity, and the need to select only a fraction of each fire's plume.

4. SMOKE EMISSION COEFFICIENTS DERIVATION

4.1 Geographic Area and Biome Delineation

This first FREM implementation focuses on southern hemisphere Africa (0.0 - 34.0° S, 8.0 - 52° E), a region showing a prolonged annual dry season (July to Sept) during which herbaceous vegetation is either dry or dormant and deciduous leaves contribute to the preponderance of fire (Archibald *et al.*, 2009). The regions wetter areas often sustain closed-canopy forests with prolonged moist conditions and heterogeneous vegetation structures that can constrain fire spread, whilst drier grasslands and more open forests and woodland savannas tend to host larger and more spatially contiguous fires, albeit with reduced accessibility to higher fuel loads. We used the GLOBCOVER 2009 landcover map (validated by Bicheron *et al.*, 2011), derived from 300 m spatial resolution ENVISAT MERIS observations, to derive our biome classification. Unlike the single 'savanna' class used by GFED and GFAS, we map grassland and woodland savanna biomes separately, as recommended by the Intergovernmental Panel on Climate Change (IPCC, 1997) guidelines for GHG emissions reporting (Korotzi *et al.,* 2004). Our aggregated landcover classes are functions of the four main GLOBCOVER vegetation structure groups of Managed Lands (including Croplands), Shrubs & Herbaceous, Grasslands, and Trees & Woody (Sophie *et al.*, 2010), and we subdivided the latter into Closed Forest and Open Forest/Woodlands (also sometimes termed woodland savanna). The resulting final five biomes we term closed forest, managed lands, shrublands, and two types of savanna - Open Forest/Woodland (woodland savanna), and Grasslands/Savanna (grassland savanna). The spatial distribution of these five biomes (shown in Fig. 3) is in fact very similar to the independently-derived Southern African woodland-grassland classification of Korotzi *et al.* (2004), derived by thresholding the MODIS percentage tree cover product (Hansen *et al.,* 2002). We derived C_{biome} coefficients for our five biomes via per-fire matchups of FRE and AOD-estimated plume mass of total particulate matter [TPM; kg].

4.2 Fire Radiative Power and AOD Datasets

Geostationary FRP data came from the EUMETSAT Land Surface Analysis Satellite Applications Facility (LSA SAF: http://landsaf.meteo.pt) Meteosat SEVIRI FRP-PIXEL product (15-min, 3 km resolution at the sub-satellite point), fully described in Wooster *et al.* (2015). Comparison to simultaneous MODIS FRP data indicates low bias on a per-fire basis, though the lowest FRP fires

(FRP ≤ 40 MW) are typically under-counted by SEVIRI compared to MODIS due to the formers larger nadir pixel area (Roberts *et al.*, 2015).

Similar to Ichoku and Ellison (2014), we used MODIS 550 nm 10 km spatial resolution AOD data (Collection 6 MOD/MYD04_L2; Levy *et al.,* 2013) to derive plume TPM. AOD's from Terra MODIS (~ 10:30 am) and Aqua (~ 1:30 pm) are generated using two retrieval algorithms, Dark Target - developed to work over dense dark vegetation, and Deep Blue - developed originally to provide coverage over brighter surfaces but now expanded to all cloud-free land. A combined AOD data layer, based on a merge algorithm, is also provided to minimise coverage gaps. FREM uses the Deep Blue output because it only needs coverage around the selected matchup fires and because these shows best agreement with southern Africa AERONET AODs (Sayer *et al.* 2014).

4.3 Fire Matchup Selection

To aid matchup selection, cloud-cover information from the LSA SAF Meteosat SEVIRI FRP-PIXEL Quality Product were used (Wooster *et al.*, 2015), along with 10 m height mean zonal wind fields from ERA interim reanalyses (Balsamo *et al.*, 2015). Cloud and wind velocity screening masks were applied to daily composites of SEVIRI FRP accumulated up to the local MODIS overpass time. Simple criteria were used to identify regions containing potential matchup fires:

(i) Cloud free conditions, to provide the FRP record of an entire fire.
(ii) Near surface winds ≥ 5 ms^{-1}, to aid generation of substantial smoke plumes.
(iii) A high total sum of SEVIRI-derived FRP (≥1000 MW) up to the time of the MODIS overpass, to ensure the presence of many potential matchup fires.

To help identify sufficiently isolated matchup fires, a series of morphological operations were also applied to the daily screened composites. These combined criteria allowed us to select a series of 500 km × 500 km target regions (Fig. 3), within which matchups were identified.

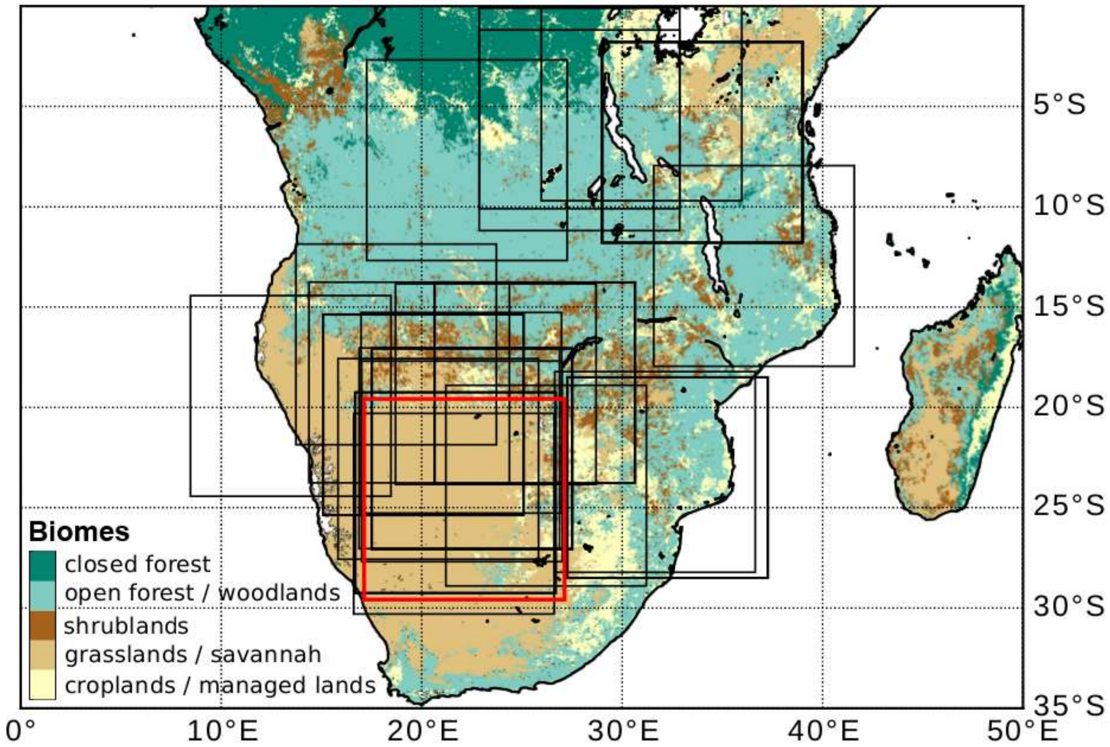

Figure 3. FREM biome map of southern Africa, based on reclassification of the GLOBCOVER 2009 landcover map and appearing similar to the woodland/grassland classification of southern Africa derived by Korontzi *et al.* (2004). Outlines show the thirty-one 500 km × 500 km target regions from which matchup fires used to generate the biome-dependent FREM smoke emissions coefficients (C_{biome}) of Fig. 7 were selected. Red outlined region has its FRP time-series shown in Fig. 4.

Each of the target regions outlined in Fig. 3 were examined across a ten-day period around the date of the identified fire activity highlighted using tests (i) to (iii) and the morphological operations described above. The FRP time-series of each region was used to identify the time of day at which fire activity was minimal, and this was used as the start time for each FRP temporal integration period to calculate the per-fire FRE, with the end time being the that of the respective Terra and Aqua MODIS AOD product used in the matchup (Fig. 4). The need to find fires whose plumes were spatially isolated from others did limit the search area/times somewhat – as some regions and periods that matched most of our criteria showed so much smoke it was difficult to isolate individual plumes. Future work will endeavour to improve on this by exploiting far higher spatial resolution AOD products, rather than the 10 km data used herein.

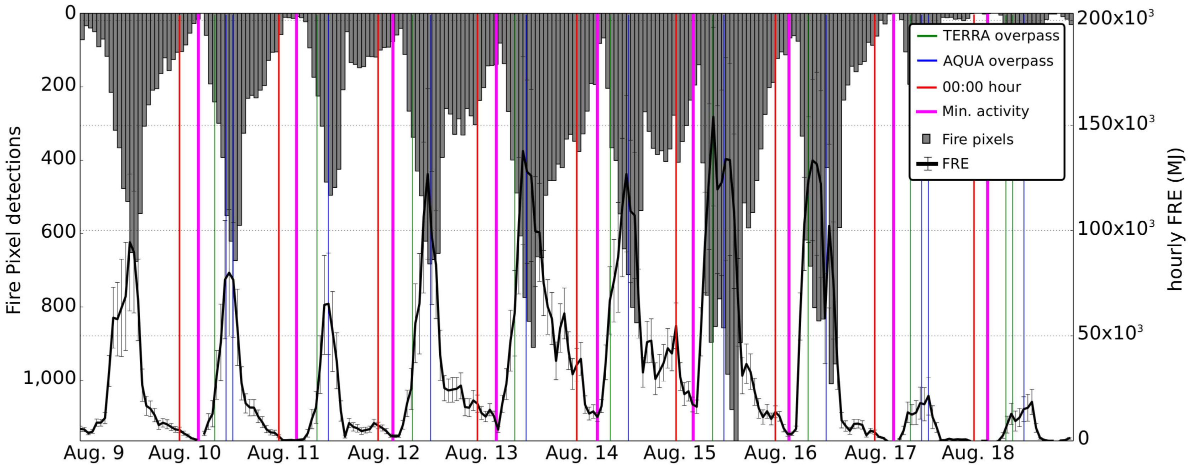

Figure 4. Time series of SEVIRI hourly active fire pixel detections (grey bins) and hourly FRE (black line) for the 500 km × 500 km region highlighted in red in Fig.3 in August 2011, located south of the Okavango Delta (see imagery in Fig. 5). Overpass times of Terra and Aqua MODIS are shown by green and blue vertical lines respectively, alongside daily solar noon (red) and the daily time of minimum fire activity minimum (magenta). Error bars on hourly FRE are calculated

from the FRP uncertainties delivered in the geostationary FRP-PIXEL product (Wooster *et al.*, 2015).

Each of the thirty-one regions, identified between July 2011 and November 2011, shown in Fig. 3, contained many candidate matchup fires, each composed of multiple active fire pixels (Fig. 5a, b). Only those for which a single GLOBCOVER class represented more than 50% of the active fire pixel locations were retained, in order to avoid burns that showed too much consumption of mixed biome vegetation. This still left hundreds of candidate fires (Fig. 5a), and for each the smoke plume was outlined and the corresponding AOD data examined (Fig. 5b, c). Fires were removed where incorrect masking of smoke as cloud had clearly occurred in the AOD products, or where non-biomass burning aerosols or surface reflectance effects seemed likely to have erroneously contributed to AOD, for example at the Etosha Pan (Namibia) or Kalahari (Botswana).

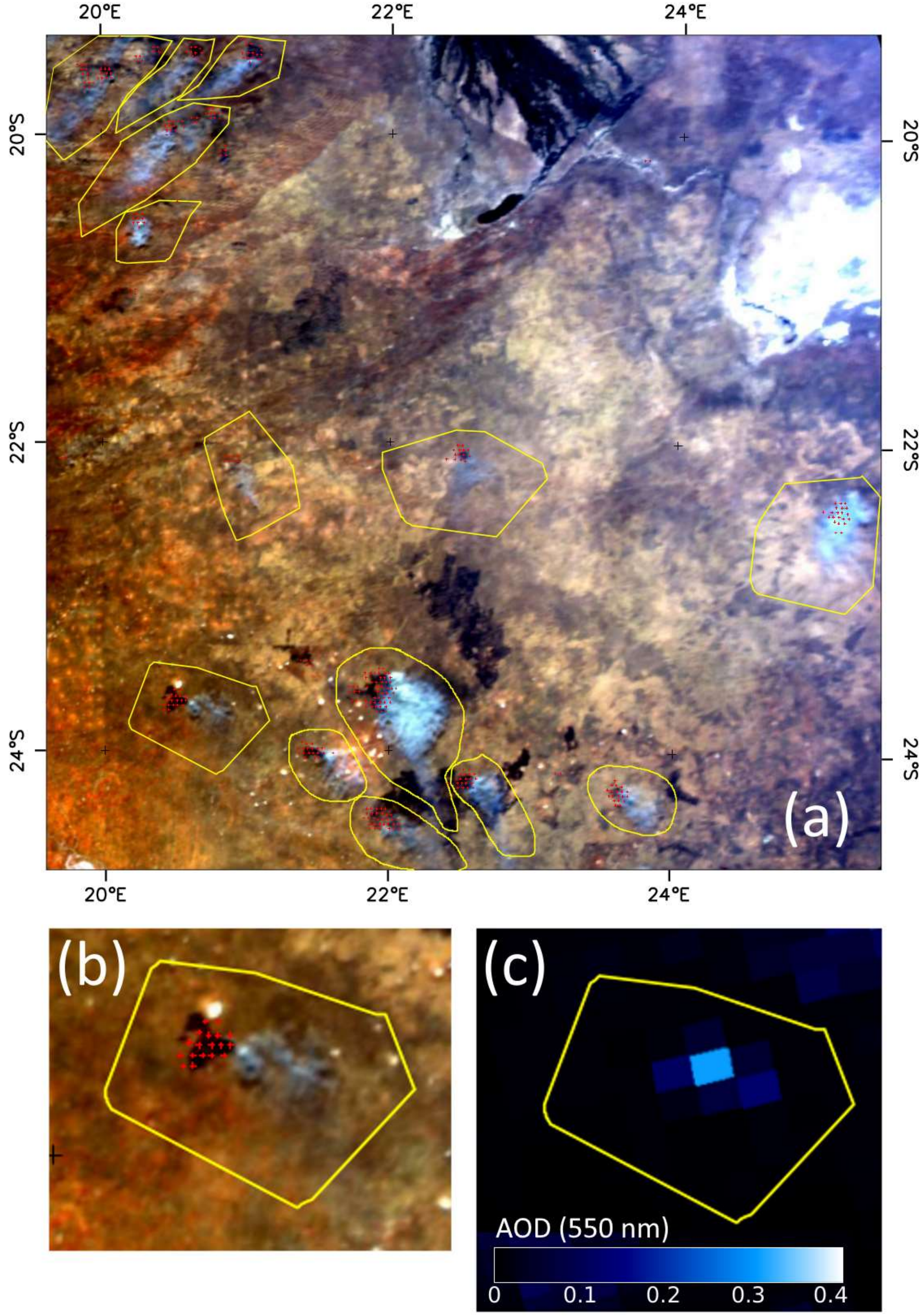
20°E
22°E
24°E
20°S
22°S
24°S
(a)
(b)
(c)
AOD (550 nm)
0
0.1
0.2
0.3
0.4

Figure 5. Example region of southern Africa from which matchup fires were selected on the afternoon of 12th Aug 2011, 12:40 UTC (MODIS Aqua overpass). (a) Region outlined in red in Fig. 3, south of the Okavango delta, depicted as a colour composite using data from the Aqua MODIS afternoon overpass [RGB=1(0.6μm), 4(0.55μm), 3(0.47μm)]. Smoke plumes from candidate active fires are outlined with yellow vectors, and the centre locations of each SEVIRI active fire pixel detected from the time of the identified active fire minimum (shown in Fig. 4) up until this Aqua overpass time are shown as red dots. (b) Zoom around the bottom left fire and plume shown in (a) to indicate detail. The dark burn scar left by the fire can clearly be seen. (c) Matching MYD04_L2 AOD data derived from the Aqua MODIS overpass shown in (b).

Each retained matchup fire had its FRE and column-integrated mass of emitted total particulate matter (TPM) estimated. The former from the temporal integration of FRP over the fire's lifetime, and the latter from the summed excess AOD (∑ΔAOD) of the outlined smoke plume, with any pixel partly or wholly encompassed by the vector included in the AOD summation (Fig. 5c and Fig. 6). All plumes were large enough to be covered by more than one 10 km AOD pixel, most by many pixels, as seen from the examples in Fig. 5 and 6. The column-integrated mass of emitted TPM was calculated following Ichoku and Ellison (2014) as the surplus 550 nm AOD above the (non-plume) AOD background (which varied over time due to e.g. smoke from prior or distant fires), multiplied by the ratio of the AOD product pixel area (m^2) to the light extinction efficiency per unit of biomass burning aerosol mass (β_e, $m^2.g^{-1}$). β_e (550 nm) was selected as 3.5 ± 1.0 $m^2.g^{-1}$, based on values listed in Table 1 for 'fresh' smoke taken from studies conducted primarily within southern Africa (plus other savanna-type fires). Ichoku and Kaufman (2005) and Ichoku and Ellison (2014) assumed a higher β_e of 4.6 $m^2.g^{-1}$, at the top end of our range, which was selected as a 'global average' applicable to plumes across all fire-affected global environments. A substantially higher 7.6 +/- 1.9 $m^2.g^{-1}$ value was assumed by Vermote et al (2005) (based on Chin *et al.* 2002), again for global aerosols and in that case not only from 'fresh' smoke. Abel *et al.* (2005) indicate β_e typically increases as smoke ages.

Table 1. Values of light extinction efficiency per unit of biomass burning aerosol mass (β_e, $m^2.g^{-1}$), also termed the smoke mass extinction coefficient, appropriate for 550 nm unless otherwise stated. A mean β_e of 3.5 ± 1.0 $m^2.g^{-1}$ was used herein, based on these studies.

β_e ($m^2.g^{-1}$)	Reference	Notes
2.22 (3.37)	Abel *et al.* (2005)	Fresh southern African biomass burning smoke (and value for 'aged' regional 'haze)
3.8 – 4.5	Reid *et al.* (2005a)	Smoke from Zambian savanna burning
4.5	Andrews *et al.* (1989)	Computed mass extinction coefficient of 'dry' smoke.
4.14 ± 1.06	Weinman et al (1981)	Savanna fires (Australia), assessed at 500 nm and assumed ~ 10% lower for 550 nm.

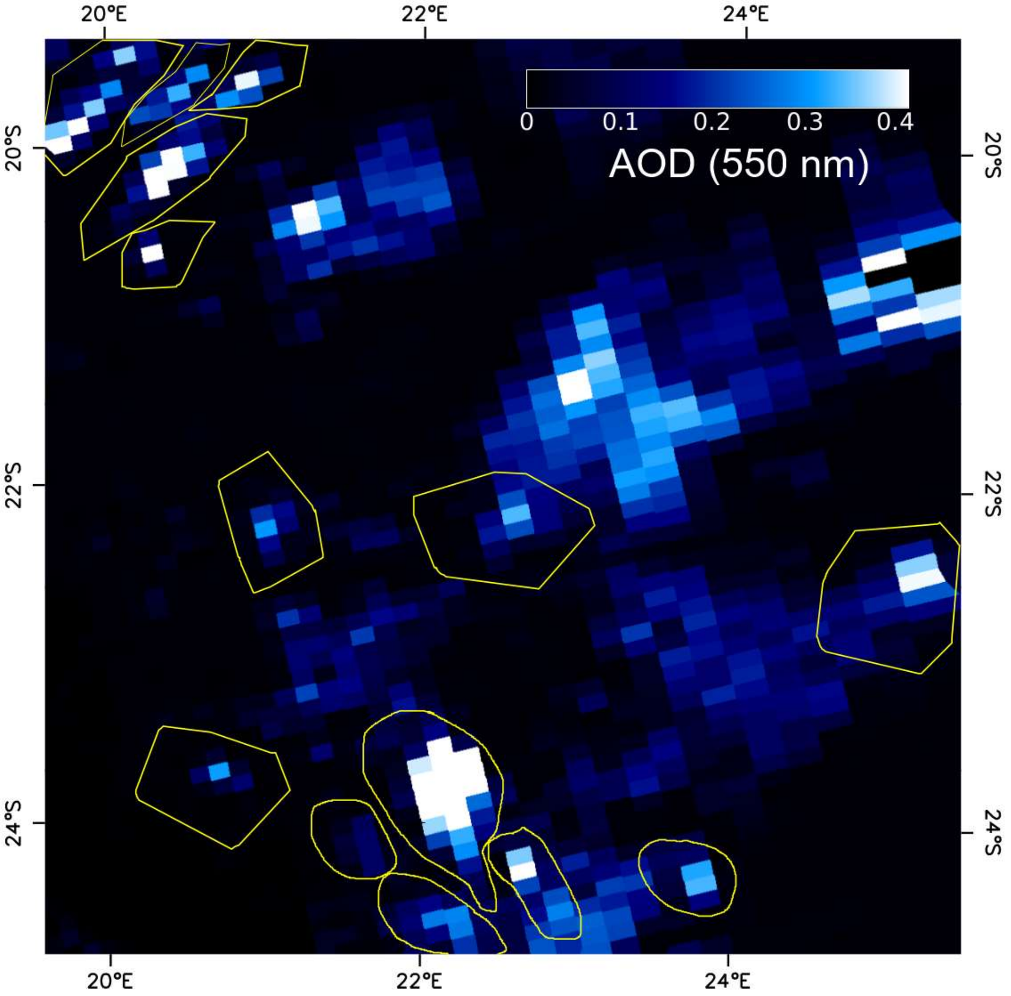

Figure 6. MODIS Aerosol optical depth (AOD) data matching the MODIS image shown in Fig. 5a. The yellow outlines from Fig. 5 here encompass the set of 10 km × 10 km MODIS AOD product pixels that are included in the plume-integrated AOD calculation for each fire. Any pixel partly or wholly encompassed by the vector is included in the AOD summation, which is then used to estimate the mass of total particulate matter in the plume. Some areas of apparently high AOD are unrelated to biomass burning and so are not outlined here, for example that immediately south of the Okavango Delta (*cf.* Fig. 5) neighbouring a highly reflective salt pan.

4.5 Derivation and Interpretation of Smoke Emissions Coefficients (C_{biome})

Final smoke emission coefficients for each biome are shown in Fig. 7 and were derived from the per-fire FRE and plume TPM matchups using linear orthogonal distance regression, which takes into account uncertainties in both datasets (Reed, 1989). Derived C_{biome} values range from 13.03 ± 0.23 g.MJ^{-1} (Grasslands) to 65.63 ± 0.91 g.MJ^{-1} (Closed Canopy Forest). Our SEVIRI-derived $C_{grassland}$ value is very similar to the laboratory derived 14.4 ± 4.3 g.MJ^{-1} determined by Freeborn *et al.,* (2008) using IR camera-derived FRP and filter-based aerosol measures, and lies towards the middle of the 10 – 19 g.MJ^{-1} range found for laboratory burns of southern African grasses (Ichoku *et al.*, 2008). Our value for Open Canopy Forests/Woodlands (19.75 ± 0.49 g.MJ^{-1}) is also similar to the 18 ± 5 g.MJ^{-1} calculated by Ichoku and Ellison (2014) for southern African savannas (Zambia), using MODIS FRP data and the FEER methodology, though our SEVIRI-derived value has significantly lower uncertainty – perhaps reflecting our more discrete land-cover classification that distinguishes Grassland Savanna from Open Forest/Woodland Savanna (Fig. 3).

Ichoku and Ellison (2014) found the MODIS-derived C_{biome} for southern African forests (D.R. Congo; 15 ± 6 g.MJ^{-1}) to be lower than that of Grassland, which is perhaps surprising since FRP observations in forests would be expected to be more affected by canopy interception of the upwelling fire-emitted thermal radiation, and forest burns also typically show greater particulate matter emissions per kg of fuel burned than do grassland burns (Akagi *et al.,* 2011). The smoke emissions coefficients for Closed Canopy Forest and Open Canopy Forest/Woodland Savanna we derive using SEVIRI and the FREM methodology (Fig. 7a, b) are, respectively, ×5 and ×1.5 what we find in Grassland Savanna (Fig. 7d), and we find this potentially more appropriate than values lower than for Grassland Savanna. We suggest similarly that tree canopy interception of upwelling surface-fire emitted FRP is likely also responsible for at least part of the higher FRE-to-fuel consumption 'conversion factor' derived for tropical forest biomes compared to savanna biomes during the calibration of GFAS v1.2 with GFED v3.1 (Kaiser *et al.*, 2012). Biome-dependent differences in the performance of GFED, for example in relation to burned area detectability (which can vary significantly between savannas, tropical forests and agricultural burning areas for example; Giglio *et al.*, 2010; Randerson *et al.,* 2012), may also play a part. By relating FRE directly to particulate matter release using emissions coefficients derived from the satellite observations themselves, FREM bypasses some of the issues affecting other fire emissions inventories, enabling it to be both fully independent of GFED and GFAS and to consider the observational characteristics of the satellite FRP measures of each biome (e.g. increasing amounts of canopy interception of upwelling fire emitted thermal radiation in biomes with a higher mean percentage tree cover).

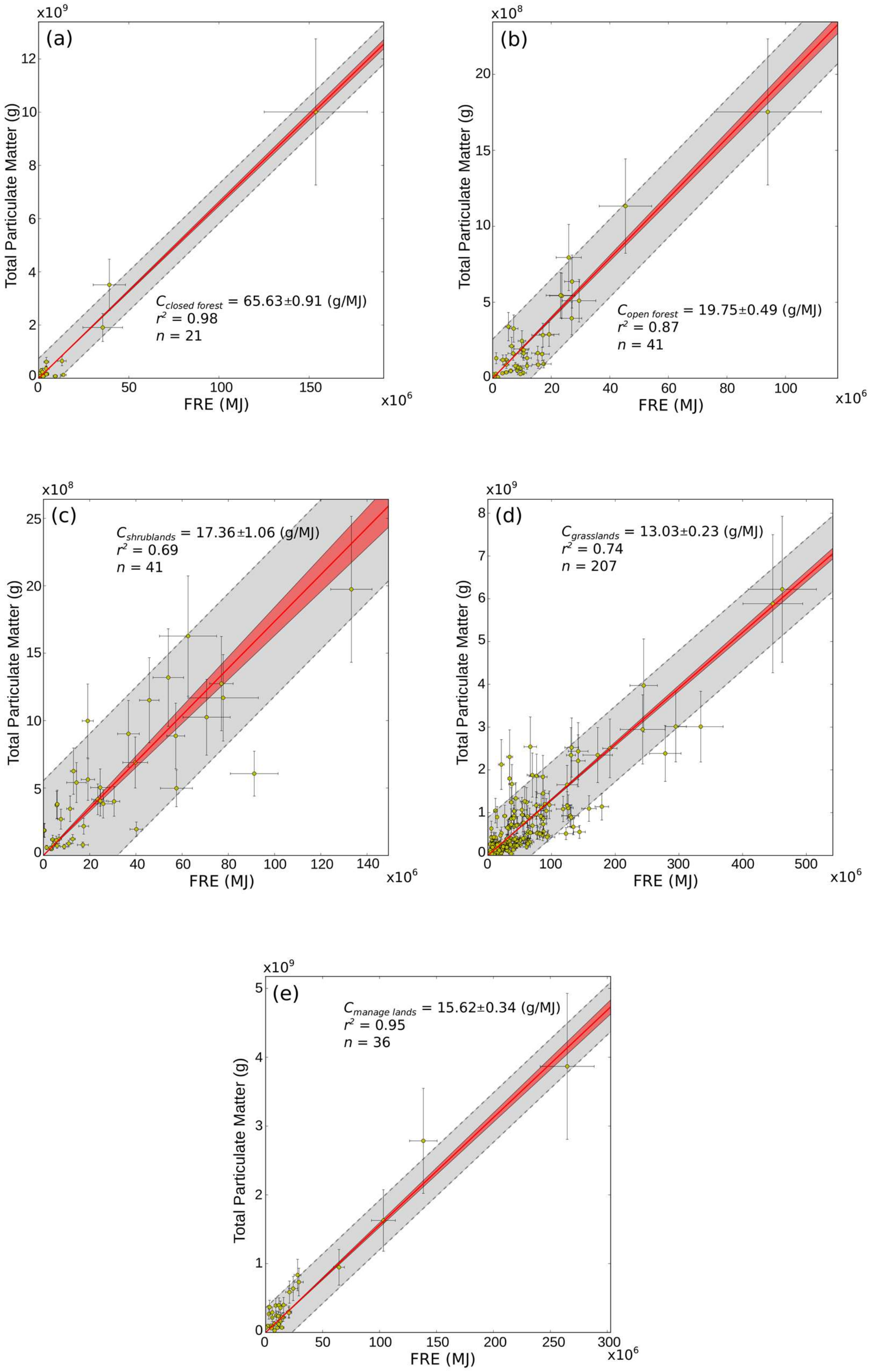
(a)
x10^9
Total Particulate Matter (g)
FRE (MJ)
x10^6
0
2
4
6
8
10
12
0
50
100
150
$C_{closed\ forest}$ = 65.63±0.91 (g/MJ)
r^2 = 0.98
n = 21
(b)
x10^8
Total Particulate Matter (g)
FRE (MJ)
x10^6
0
5
10
15
20
0
20
40
60
80
100
$C_{open\ forest}$ = 19.75±0.49 (g/MJ)
r^2 = 0.87
n = 41
(c)
x10^8
Total Particulate Matter (g)
FRE (MJ)
x10^6
0
5
10
15
20
25
0
20
40
60
80
100
120
140
$C_{shrublands}$ = 17.36±1.06 (g/MJ)
r^2 = 0.69
n = 41
(d)
x10^9
Total Particulate Matter (g)
FRE (MJ)
x10^6
0
1
2
3
4
5
6
7
8
0
100
200
300
400
500
$C_{grasslands}$ = 13.03±0.23 (g/MJ)
r^2 = 0.74
n = 207
(e)
x10^9
Total Particulate Matter (g)
FRE (MJ)
x10^6
0
1
2
3
4
5
0
50
100
150
200
250
300
$C_{manage\ lands}$ = 15.62±0.34 (g/MJ)
r^2 = 0.95
n = 36

Figure 7. Biome dependent smoke emissions coefficients (C_{biome}, g.MJ^{-1}) derived from the slope of the linear best fit made between the amount of total particulate matter in a plume (grams) and the amount of radiative energy released by the causal fire (FRE, MJ). Red shaded area represents the 95% confidence interval on this slope (i.e. the uncertainty in C_{biome}), whilst the grey shaded area represents the prediction interval (i.e. the interval encompassing to 95% probability the value of TPM given a single value of FRE). Coefficients are shown for the biomes of (a) Closed Canopy Forest, (b) Open Canopy Forest and Woodland (Woodland Savanna), (c) Shrublands, (d) Grasslands (Grassland Savanna), and (e) Managed lands (including Croplands). For each biome, each data point represents a single fires FRE calculated from a series of Meteosat FRP-PIXEL products (Fig. 4), and specifically from the fire activity minimum up until the time of the satellite overpass from which the matching smoke plume TPM was estimated from the MODIS AOD product (Fig. 5; Fig. 6). Uncertainties in FRE (1σ) are derived from the FRP-PIXEL uncertainty metrics (Wooster *et al.*, 2015), whereas those in TPM are derived from the ±1.0 m^2.g^{-1} uncertainty in the assumed smoke aerosol extinction cross-section (Table 1) and the MODIS AOD uncertainty layer. MODIS AOD uncertainties estimates correspond to one-standard-deviation Gaussian confidence interval of the envelopes resulting from the comparison of retrieved AOD data and AERONET measures. These depend on the AOD, QA flag, and viewing geometry (Sayer *et al.,* 2013).

5. APPLICATION TO EMISSIONS INVENTORY DEVELOPMENT

5.1 Emissions of Total Particulate Matter (TPM)

The smoke emissions coefficients derived in Section 4 were applied to hourly averages of the Meteosat SEVIRI FRP-PIXEL products described in Wooster *et al.* (2015), thus calculating pixel-based TPM emissions rates ($g.hr^{-1}$). To account for the fact that each SEVIRI pixel can contain more than one biome – especially in fragmented areas and transition zones - the fractional coverage of each of our five biomes was calculated for each pixel, and the relevant area weighted average smoke emissions coefficient used. Coefficients were in fact applied to three versions of the FRP-PIXEL data - (i) the basic FRP observations made at the native SEVIRI spatial resolution, (ii) those adjusted by the cloud cover fraction (δ) stored in the matching FRP-GRID product (5° resolution), and (iii) those adjusted by cloud-cover fraction and an additional factor accounting for under-counted 'small' (i.e. low FRP) fires at or below the nominal SEVIRI FRP minimum detection limit. Each FRP dataset is fully detailed in Wooster *et al.* (2015). Fig. 8 shows the resulting monthly FREM-derived time-series of TPM emissions, alongside those of GFEDv4.1s (Van der Werf *et al.*, 2017; www.globalfiredata.org/), GFASv1.2 (Kaiser *et al.*, 2012; www.gmes-atmosphere.eu/about/project_structure/input_data/d_fire/) and FEERv1.0-G1.2 (Ichoku and Ellison, 2014; www.feer.gsfc.nasa.gov/data/emissions/). Differences between FREM monthly 'raw' and 'cloud adjusted' TPM emissions are typically low and within the uncertainty of the 'raw' estimates alone throughout most fire seasons (except late season 2009), indicating that most fires in southern Africa typically burn far away from significant cloud cover. FREM's mean cloud adjusted TPM emissions are (1.96 ± 0.39) x10^7 $Tg.year^{-1}$, 45% higher than GFAS v1.2 and 12% higher than GFED v4.1s (which already includes a substantial upward adjustment for fires whose burned area is too small to be detected by MODIS; Van der Werf *et al.*, 2017), but lower than those of FEER by a margin of ~ 30%.

The TPM emissions distribution between the different biomes is shown in Table 2, and for the peak fire months of July/August, mean FREM cloud-adjusted TPM emissions are 50% higher than GFAS, 27% lower than those of FEER, and 12% higher than GFED v4.1s. The GFED burned area and/or fuel consumptions per unit area would overall therefore need to be increased by relatively minor amounts for the resulting emissions to match those of FREM – though when FREM emissions are adjusted for the low FRP component of the regions fire regime - which is undetectable by SEVIRI but detectable by MODIS (shown by e.g. Freeborn *et al.*, 2009) – FREM's mean annual TPM emissions increase more substantially above GFED v4.1s (to an average of 64%), with an even higher difference when compared to GFAS v1.2 (Fig. 8). These cloud-adjusted FREM emissions of total particulate matter are, however, within 1% of those provided by the MODIS FRP-based FEER inventory.

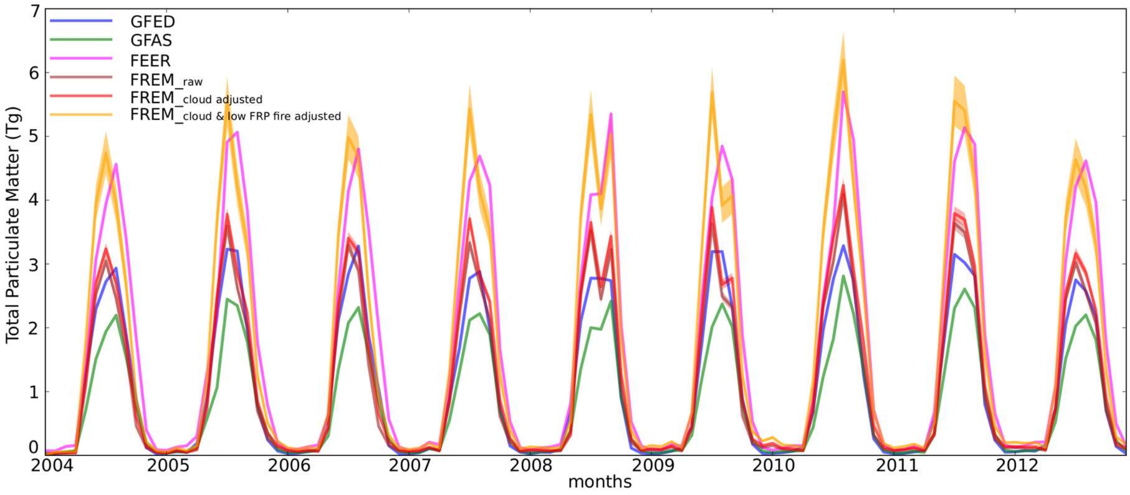

Figure 8. Monthly total particulate emissions estimates for southern African fires, derived from the FRE$_{\text{emissions}}$ methodology (FREM) applied to the SEVIRI FRP-PIXEL product of Wooster *et al.* (2015) for 2004-2012. Three versions are shown, those based on 'raw' SEVIRI FRP observations, those adjusted for cloud cover, and those adjusted for 'cloud cover and under-detected low FRP fires' (see Section 5.1 and 5.2). The associated uncertainties are shown in each case. Corresponding TPM emissions from the GFED v4.1s, GFAS v1.2 and FEER v1.0 inventories

are shown for comparison, and the cloud and low FRP fire adjusted FREM values calculated from SEVIRI lie very close to the MODIS-derived FEER estimates.

Table 2. Emissions of total particulate matter (TPM; Tg) per year across southern Africa, as calculated using the FREM approach (Cloud and low FRP adjusted version), along with the percentage contributed by the different biome types of Fig. 3.

		% of TMP Emissions in a Biome				
	Annual TPM Emissions (Tg)	**Closed Forest**	**Shrublands**	**Croplands / Managed Lands**	**Open Forest / Woodland Savanna**	**Grassland Savanna**

2004	14.7	23.4	14.0	11.3	45.3	5.9
2005	16.1	25.3	13.9	12.0	42.6	6.3
2006	14.4	25.5	13.1	11.5	43.5	6.3
2007	16.2	24.0	14.0	12.2	42.0	7.8
2008	17.4	25.6	13.4	12.4	40.4	8.2
2009	16.1	25.4	13.3	11.5	42.8	6.9
2010	19.3	25.1	13.2	12.5	39.5	9.8
2011	17.3	22.6	14.1	11.8	38.0	13.5
2012	15.6	25.0	13.8	11.5	39.9	9.9

5.2 Low FRP Fire Adjustment

As seen in Fig. 8, the ‘low FRP fire’ adjustment (Wooster *et al.,* 2015) increases FREM’s TPM emissions substantially compared to the ‘cloud-adjusted’ values alone. Freeborn *et al.* (2009; 2014) describe in detail the bias adjustments needed to be made to SEVIRI’s FRP data when deriving total FRP or FRE metrics, which are required to account for low FRP fire pixels below the SEVIRI minimum FRP detection limit. At the scales used here, a simple 46% upscaling delivers a SEVIRI-derived FRP dataset with very low bias (~ 2%) compared to simultaneous MODIS FRP observations (Roberts *et al.*, 2015), and this adjustment is included here. However, with the FREM approach it is possible that the adjustment should be of a smaller magnitude. This is because, whilst the generally high FRE fires used for the smoke emissions coefficient derivation (Fig. 7) have their FRP very well measured by SEVIRI at the time of the afternoon MODIS overpass, with only a 3 MW mean bias seen in southern Africa (Roberts *et al.*, 2015), earlier in their lifetime these fires will likely have included areas burning below SEVIRI's minimum FRP detection limit but whose smoke will have contributed to the AOD of the matching plume. Thus the resulting smoke emissions coefficient will already likely account for some of the impact of fire pixels burning below the SEVIRI sensors minimum FRP detection limit, though the extent of this is unknown at present. For now therefore, the 46% upward adjustment used in the FRP-GRID product (Wooster *et al.,* 2015; Roberts *et al.,* 2015) is also applied in FREM as the 'low FRP fire' adjustment

5.3 TPM Emissions Interpretation

Outputs from FREM (cloud- and low-FRP fire adjusted) agree very well with those of FEER, are very significantly higher than those of GFAS (factor of ×2.2), and are also higher than GFED (against which GFAS is calibrated) (Fig. 8). The implication that GFAS may significantly underestimate of TPM emissions across southern Africa agrees with Kaiser *et al.* (2012), who found GFAS's southern African aerosol emissions required a ×3 upward scaling to replicate AOD observations. Those of GFEDv3.1 (whose carbon emissions for southern Africa are around 20% lower than GFEDv4.1s used here) are reported to require a ×2 upscaling (Tosca *et al.*, 2013), and

Reddington *et al.* (2016) report need for similar upscalings based on an alternative aerosol model. FREM cloud- and low-FRP fire adjusted emissions therefore appear more consistent with TPM emissions totals stated to reproduce satellite AOD's in southern Africa than are those of GFAS and GFED.

In addition to differences in magnitude, Fig. 8 also indicates timing differences between emissions inventories. Across the nine years, FREM shows maximum TPM emissions in July - except for August in 2010 - and GFED an almost even split between these two months. FEER shows peaks in August (apart from 2008 in Sept), as does GFAS (apart from 2008 again in Sept, and in 2005 July). To help explore the reasons, Fig. 9 depicts for 2012 the percentage of daily FRE measured by SEVIRI that is released (a) during the two-hour window surrounding the four daily MODIS overpasses, and (b) by fires in each of the five biomes. Daily FRE (grey line) is high throughout most of June to August, and the proportion of daily FRE released around the MODIS overpass time also remains reasonably constant (Fig. 9a), with both starting to decrease more significantly from mid-September onwards. The July and August differences in month of maximum TPM emissions between FREM (which uses geostationary FRP) and FEER and GFAS (which both use MODIS FRP) seem therefore not to be due to a significantly changing fire diurnal cycle with respect to MODIS' sampling times. Fig. 9b indicates however that a significant shift in the biomes being most affected by fire occurs between July and August, with an increase in the proportion of total FRE released in Grassland Savannas with respect to Open Forest/Woodland Savannas. In FREM, the smoke emissions coefficient for Grasslands is significantly lower than that of the higher fuel load Open Forest/Woodlands (Fig. 7), which is identifiable only because our biome classes discriminate between these two savanna types as recommended by IPCC (1997). Other fire emissions inventories predominantly classify these as a single biome, and so are largely invariant to the distinction. FREM’s more discrete biome mapping appears to be the primary reason that it reports TPM emissions decreasing from July to August, because more of the fires are burning in grassland savanna biomes dominated by finer fuels whose emissions contain, on average, less particulate matter per unit of fuel consumed compared to more wooded savanna areas. Going into September, a diurnal cycle change does appear to occur, as the percentage of total radiative energy released during the MODIS overpass times decreases more markedly than during the two prior months (Fig. 9a), and the proportion of fires in grasslands and managed lands increases (Fig. 9b).

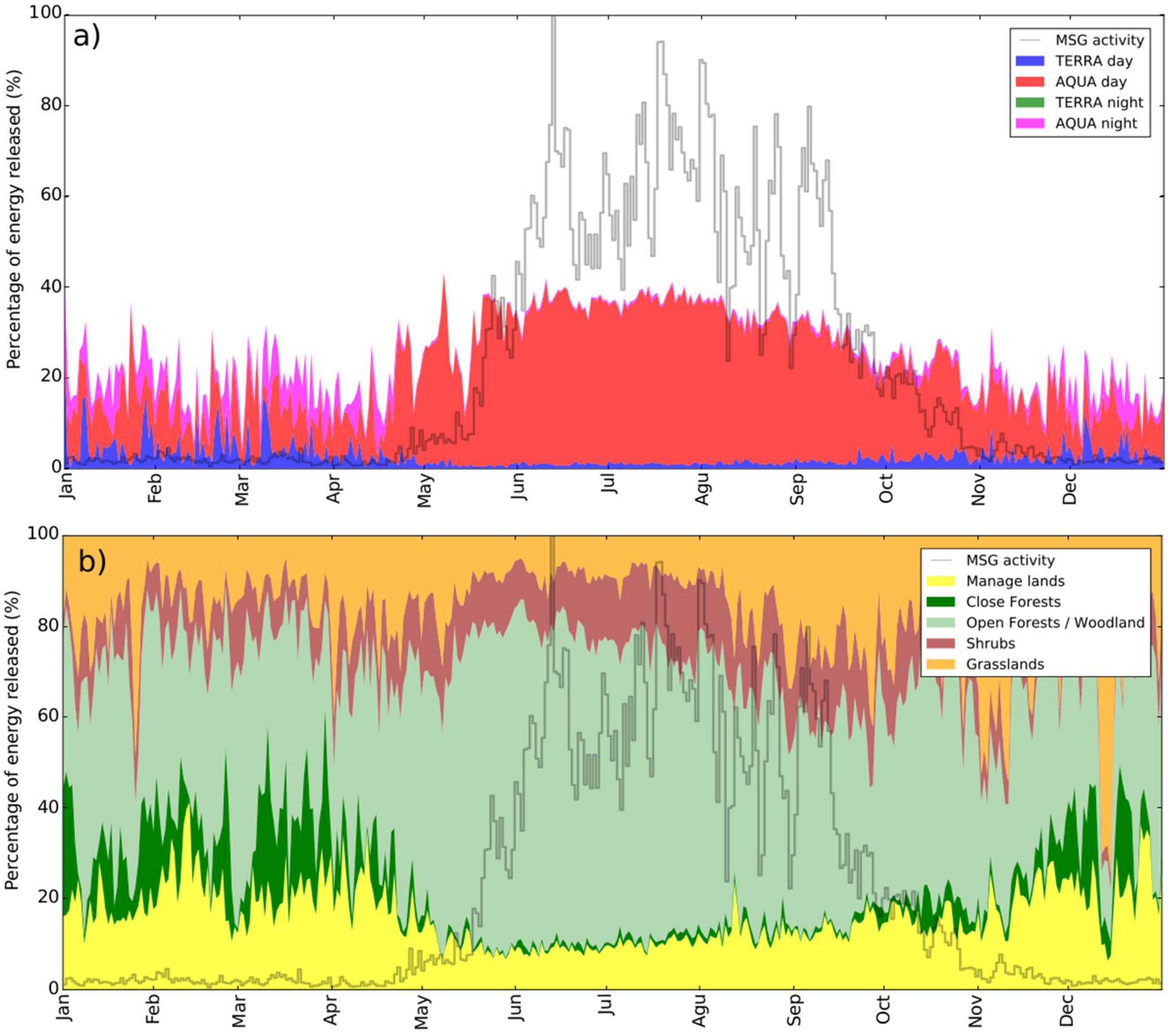

Figure 9. Percentage of daily FRE calculated from the Meteosat SEVIRI FRP-PIXEL product for 2012 that is released (a) during the ± 1 hr window encompassing the MODIS overpass time, and (b) in each biome. For comparison to the percentage values, fire activity expressed as daily FRE from MSG SEVIRI is also shown (grey line, scaled from 0 to 100%).

5.4 Comparison to GFEDv4.1s

To explore in more detail per-biome TPM emission differences between FREM and GFED4.1s, Figure 10 shows the cumulative sum of FREM's emissions as a function of the ratio of those of FREM to GFED4.1s (calculated for GFEDs 0.25° grid cells and for both cloud adjusted FREM (Fig. 10a) and cloud and low FRP fire adjusted FREM (Fig. 10b)). Discounting adjustment of the TPM emissions factor, this ratio describes the change required to the GFEDv4.1s burned area and/or or fuel consumption per unit area measure of a grid cell such that the cells TPM emissions would equal those of FREM. Taking the Open Forest/Woodland Savanna biome first (which is responsible for over half of the overall TPM emissions; Fig. 9b), Figure 10a shows that in the cloud-corrected FREM inventory, 26% of emissions are accounted for by grid cells where FREM's emissions are lower than GFEDv4.1s (i.e. FREM-to-GFED TPM ratio < 1.0), with a further 33% having a ratio in the range 1.0 to 1.5. For these cells, GFED burned area × fuel consumption per unit area metric would need to decrease or increase by a maximum of 50% for their emissions total to equal that of FREM (noting that GFED will have classed some of the cells as different biomes compared to FREM, and using only a single savannah class). Open Forest/Woodland Savanna cells needing more than a doubling of GFED4.1s burned area × fuel consumption per unit area are responsible for only a small fraction (~ 10%) of the biomes FREM emissions. The equivalent figures for other biomes can be extracted from Fig. 10a, and in order of their overall TPM emissions totals, the biomes of Open Forest/Woodland Savanna, Grassland Savanna, Managed

Lands and Shrublands show FREM TPM emission estimates 1.1, 2.3, 1.2, and 1.4× higher than GFED4.1s respectively, whereas Closed Forests are lower (0.7×). Overall, FREM's cloud-adjusted TPM emissions are 12% higher than GFED4.1s, but adjustment for low FRP fires increases the above ratios by a factor of 1.46 and substantially increases overall FREM TPM emissions above GFED4.1s (see Section 5.1), resulting in a consequent increase in the per-grid cell ratios as well (Fig. 10b).

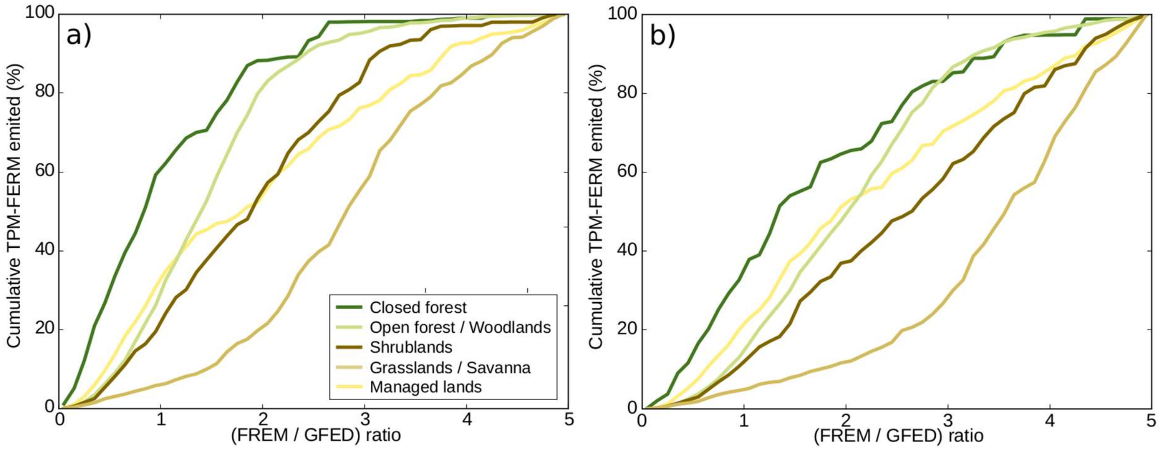

Figure 10. Cumulative sum of FREM-derived TPM emissions (%), expressed as function of the per-grid cell FREM-to-GFED v4.1s emissions ratio. Calculations were performed using the 0.25° grid cells of GFED, and 85% of cells had non-zero values in both inventories. < 1% of cells had a non-zero Colours are the same as those mapped in Fig. 3. (a) shows the results using the cloud-corrected FREM, and (b) the cloud and low FRP fire corrected FREM.

5.4 High Spatio-Temporal Resolution Emissions Estimates

Fig. 11 shows FREM's hourly TPM emission rate [kg.hr^{-1}] for 2012, the corresponding daily mean rate [kg.day^{-1}] and those of GAFSv1.2 and FEERv1.1, and the equivalent daily mean rate calculated from the GFEDv4.1s monthly values. Note that GFEDv4.1s day-by-day estimates are also available via scaling of the monthly GFED totals with numbers of active fire detections made per day across the month (van der Werf *et al.,* 2017). As with monthly totals (Fig. 8), FREM's daily TPM emission rates (cloud and low-FRP fire adjusted) are very similar to those of FEER, whilst those of GFED and GFAS are substantially lower - apparently unrealistically so as already discussed by Kaiser *et al.* (2012), Tosca *et al.* (2013) and Reddington *et al.* (2016). In addition to the apparently more representative magnitudes, the potential value of the very high temporal resolution emissions estimates offered by FREM is clear from the fact that hourly rates peak at more than 500% of the daily means. Fig. 12 provides more detail of this for August 2012, illustrating the very strong emissions diurnal cycle, and this temporal detail may become particularly important when linking emissions to atmospheric chemical transport models (e.g. Hyer *et al.*, 2007; Baldassarre *et al.*, 2015; Roberts *et al.*, 2015).

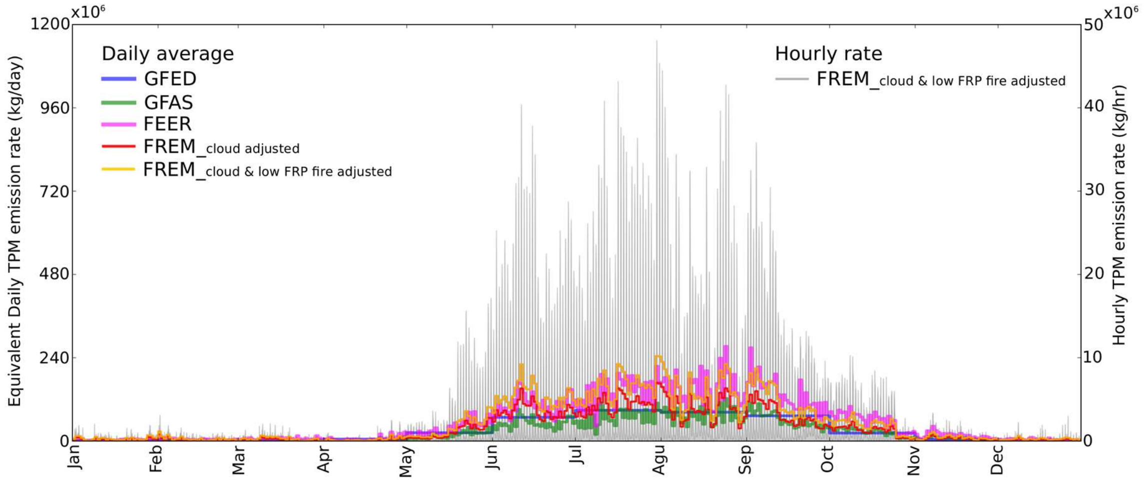

Figure 11. Emission rates of total particulate matter (TPM) coming from landscape fires in 2012 across southern Africa, as derived from the FREM methodology applied to SEVIRI FRP-PIXEL data, and from GFEDv4.1s, GFASv1.2 and FEERv1.1. GFAS and FEER provide daily values, and GFED monthly values. All are shown as equivalent daily mean rates for comparison, but the FREM-derived values can be calculated at up to 15-min temporal resolution direct from the SEVIRI FRP observations. In addition to FREM daily means, FREM-hourly averages are therefore also shown (rhs y-axis), and these show far higher daytime peaks than the daily averages.

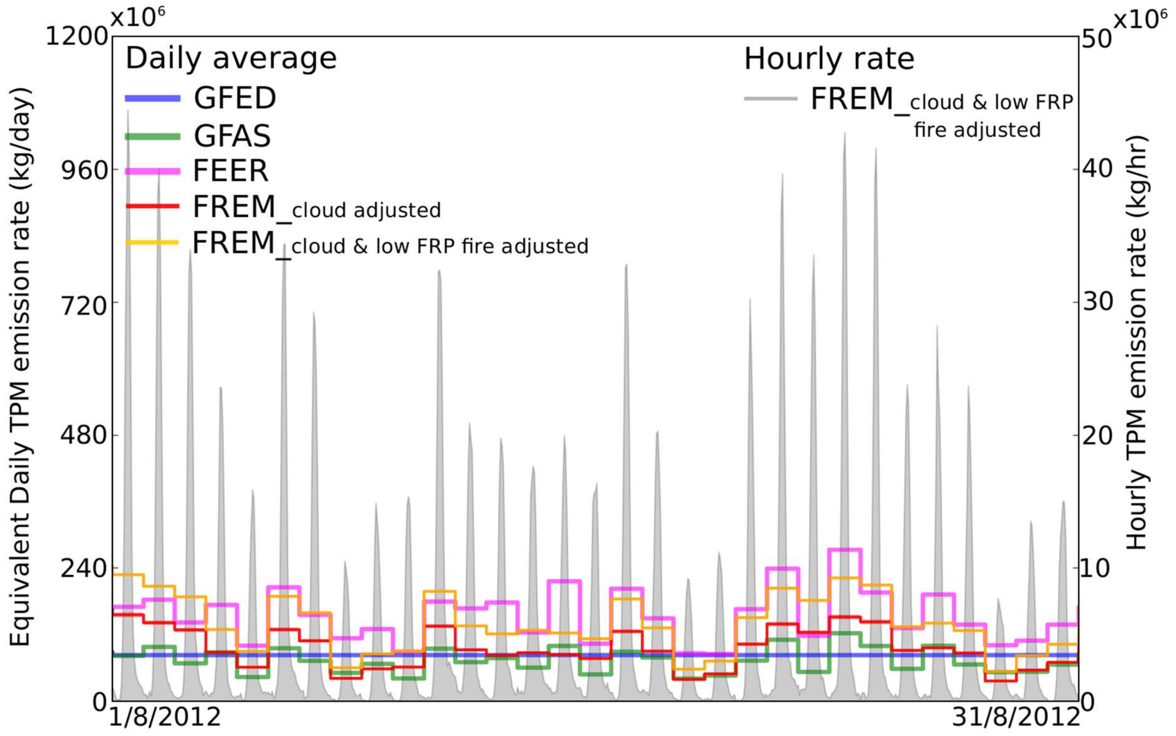

Figure 12. Data of Fig. 11 shown only for August 2012 to see more detail, particularly of the strong diurnal variability in TPM emissions enabled by the FREM approach.

In addition to its very fine temporal resolution, FREM can operate at the full spatial resolution of the original FRP observations, which for SEVIRI coarsens to around 0.05° over southern Africa. The 625×, 25× and 25× smaller pixel area than the grid cells of GFED, GFAS and FEER respectively leads to far finer-grained definition of smoke emission sources (Fig. 13), though the overall spatial patterns of FREM's emissions sources broadly agrees with the other inventories (Fig. 14).

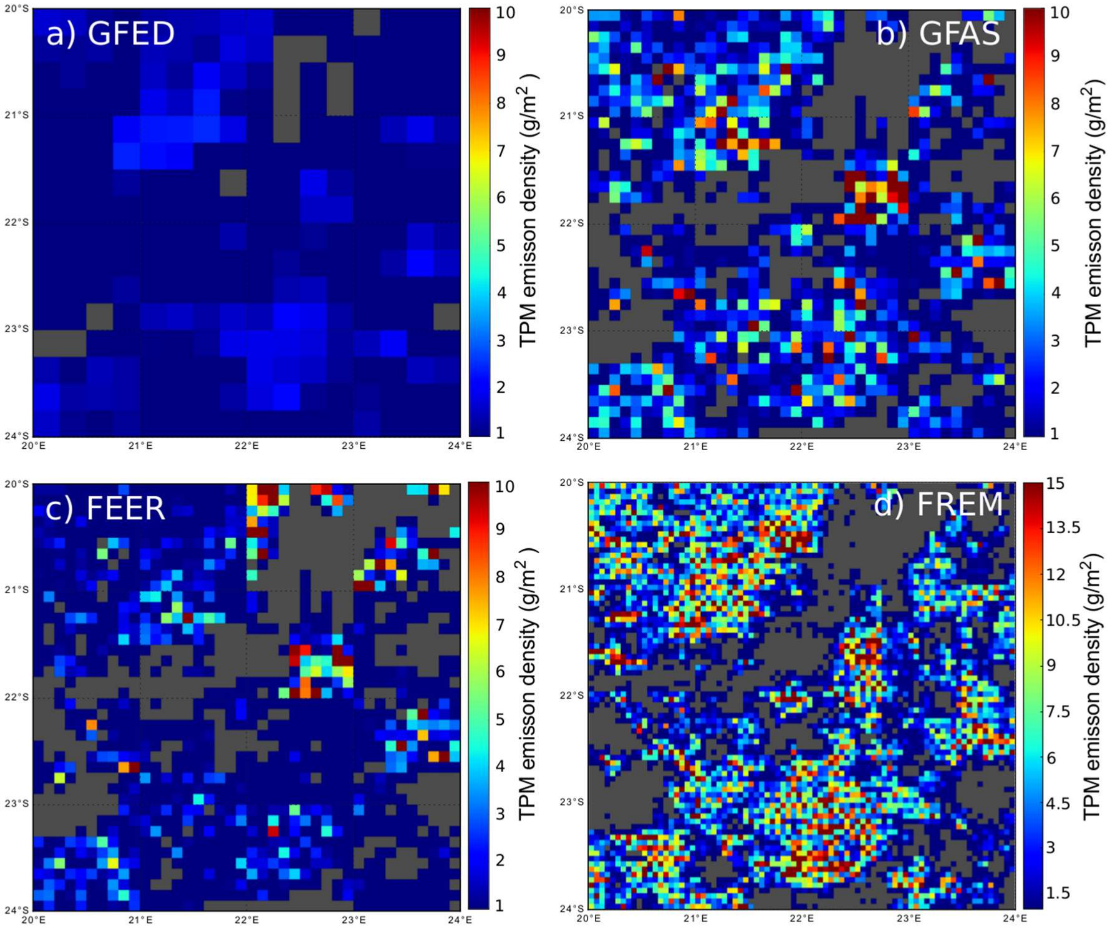

Figure 13. Total particulate matter (TPM) emission density (g.m^{-2} equivalent averaged over each grid cell) for the 25,000 km^2 area of southern Africa outlined in red in Fig. 3 for 2011, as depicted by (a) GFEDv4.1s (0.25° grid cells), (b) GFASv1.2 (0.1° grid cells), (c) FEERv1.1 (0.1° grid cells)

and (d) FREM inventory (0.05 ° grid cells). The coarser the grid resolution typically the lower the emission density values, since many of the fires typically do not cover entire cells, particularly for the coarser-scale inventories. Results for the FREM cloud and small fire adjusted inventory are shown in (d), with a different colour-bar than for the other inventories. Values for the cloud-adjusted FREM inventory can simply be provided by using the colour bar shown in (a), (b) and (c) also for (d).

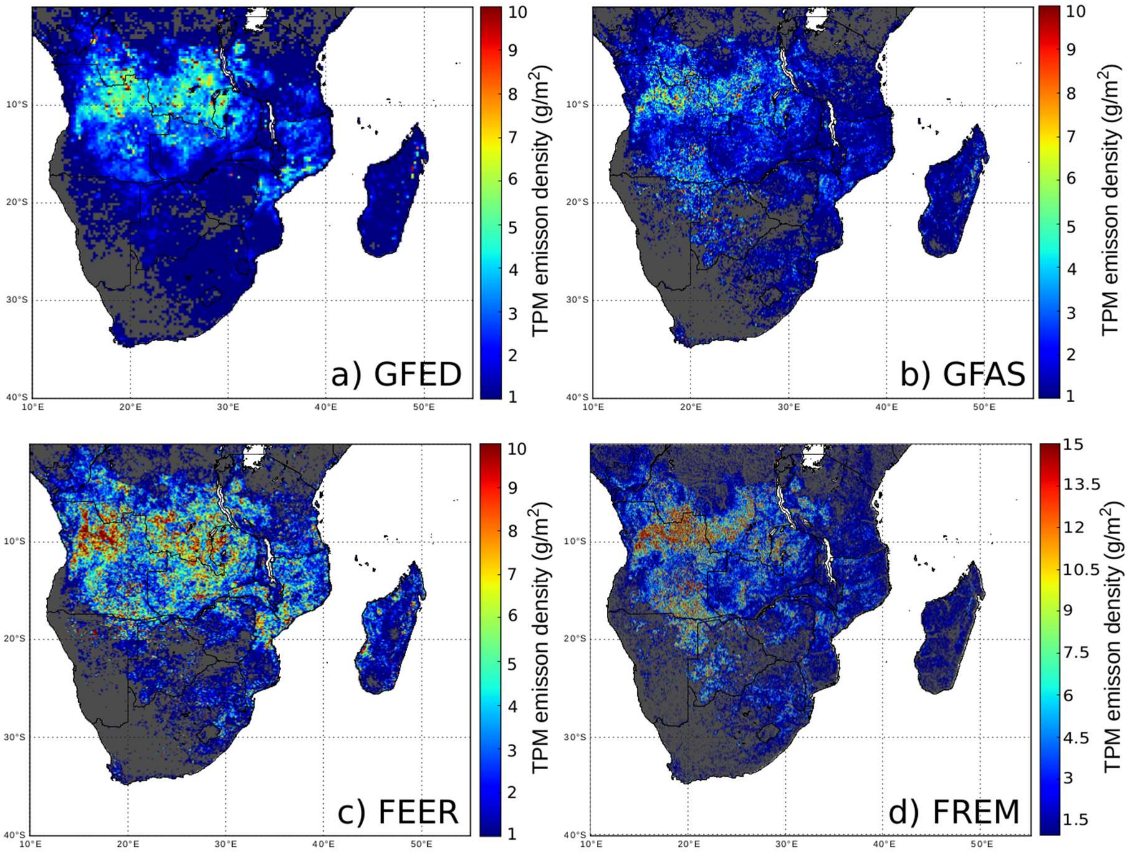

Figure 14. Total particulate matter (TPM) emission density (g.m^2) across all of southern Africa in 2011, as depicted by (a) GFEDv4.1s (0.25 ° resolution), GFASv1.2 (0.1 ° resolution), FEERv1.1 (0.1 ° resolution) and the SEVIRI FRP-derived FREM inventory (0.05 ° resolution). See Fig. 13 and its caption for more detail, and note the differing colour bar of (d).

6. TRACE GAS & CARBON EMISSIONS, AND FUEL CONSUMPTION PER UNIT AREA

6.1 Trace gas Emissions Methodology

Trace gas emissions are estimated in FREM using standard gaseous emissions factors (EF_{GAS}), but applied in a different way to in GFED and GFAS, where they are multiplied by the calculated total fuel consumption (or fuel consumption rate) to estimate total emissions (or emissions rates). Within FREM, trace gas fluxes are instead calculated via direct multiplication of the FRP data by a set of gaseous emissions coefficients, avoiding the intermediate fuel consumption step. These coefficients are calculated via multiplication of the TPM emissions coefficients (Fig. 7; Table 3) and the relevant particulate and trace gas emissions factor ratios (i.e. the ratio of EF_{GAS} to EF_{TPM}), similar to how Huijnen *et al.*, (2016) estimated CO_2 and CH_4 releases from SE Asian fires from optimised estimates of fire-emitted CO. As with the EFs themselves, EF ratios vary markedly by biome, and here we used EF's from Andreae and Merlet (2001) - as do GFED and GFAS - to calculate the gaseous emissions coefficients (g.MJ^{-1}) listed in Table 3.

Table 3. Trace gas smoke emission coefficients (and their uncertainties), derived using the ratio of the relevant trace gas emissions factor to total particulate matter emissions factor (g.kg^{-1}.g.kg^{-1}) and the smoke emissions coefficients (g.MJ^{-1}) for total particulate matter (TPM) shown in Fig. 7 (repeated in the Table). The emissions factors used in the calculation, taken from updates to Andreae and Merlet (2001) presented in Kaiser *et al.* (2012) are also shown. Note the smoke emissions coefficient represents 'emissions (g) per unit of SEVIRI-observed FRE (MJ)'. Use of geostationary sensors, such as the forthcoming Meteosat Third Generation (MTG), that have a minimum FRP detection limit different than that of SEVIRI (Freeborn *et al.*, 2009; 2014) may result in the need to derive updated coefficients.

	Species Emission Coefficient ± uncertainty (g.MJ^{-1}) Species Emissions Factor (g.kg^{-1})				
	Closed Canopy Forest	Open Canopy Forest/Woodland	Shrubland	Savanna Grassland	Managed Lands
TPM	65.6 ± 0.9 11.8	19.8 ± 0.5 8.5	17.4 ± 1.0 8.5	13.0 ± 0.2 8.5	15.6 ± 0.3 8.5
CO_2	9044 ± 2506 1626	3825 ± 1460 1646	3361 ± 1296 1646	2523 ± 962 1646	3024 ± 1154 1646
CO	562 ± 189 101	142 ± 71 61	125± 64 61	94 ± 47 61	112 ± 56 61
CH_4	36.7 ± 19.4 6.6	5.1 ± 2.8 2.2	4.5 ± 2.5 2.2	3.4 ± 1.9 2.2	4.0 ± 2.2 2.2

6.2 Trace Gas Emissions Results

FREM's CO_2, CO and CH_4 emissions estimates (Fig.14a) show the same seasonal characteristics as those of TPM, with temporal peaks in accordance with GFED. In terms of CO, Pechony *et al.* (2013) report that GFED appears to underestimate emissions in the southern hemisphere, and report the strong influence of the diurnal cycle, with afternoon CO emissions being around double those estimated from the morning overpass of MOPITT. This attests to a potential advantage of the high temporal resolution FREM inventory. Kopacz *et al.* (2010) also report a roughly factor of two difference between GFEDv2 CO emissions for southern Africa and those estimated from adjoint atmospheric inversion of satellite CO observations. Comparison of Van der Werf *et al.* (2010) and http://www.globalfiredata.org/) shows a decrease in CO emissions for southern Africa from GFEDv2 to GFEDv4.1s, so the latter appears still to deliver CO emissions lower than satellite CO data may imply. The cloud-adjusted FREM inventory indicates CO emissions 11% and 44% higher on average than GFEDv4.1s and GFASv1.2 respectively, with much larger differences when the low-FRP fire FREM adjustment is included and CO flux magnitudes become very similar to those of FEER (Fig. 14). Similar relationships are seen for CH_4 and CO_2, and the flux of any other trace gases can be easily derived within the FREM framework via the application of the relevant emissions factor ratios.

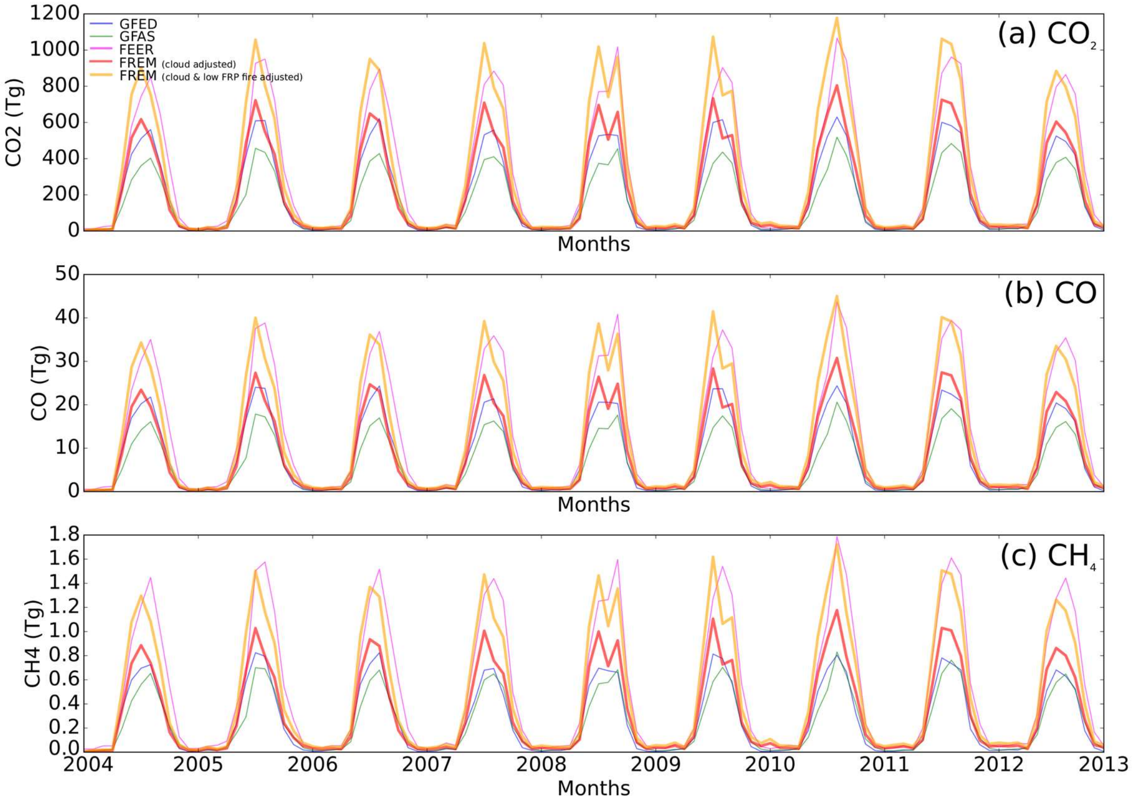

Figure 15. Monthly emissions (Tg) of CO_2, CO and CH_4 for southern Africa (2004-2012) for the FREM inventory, along with those of GFEDv4.1s, GFASv1.2 and FEERv1.1.

6.2 Total Carbon Emissions and Fuel Consumption

Since CO_2, CO and CH_4 are responsible for ~ 99% of carbon emitted by southern African landscape fires (Delmas *et al.*, 1995; Keene *et al.*, 2006), summation of their carbon allows for derivation of total C-emissions. By making the normal assumption that vegetation is 50 ± 5% carbon, landscape-scale total fuel consumption can then be estimated - for the first time from a fully ‘top down’ approach. Temporal trends in total C emissions replicate those seen in CO_2 (Fig. 15a), with mean (± 1σ) annual C-emissions of 710 (± 61) Tg calculated for southern Africa across the nine years of study (range of 213 Tg), rising to 1038 (± 88) Tg when the low FRP fire adjustment is included. Total fuel consumption is simply calculated as twice the carbon emissions, and is 12% higher than GFEDv4.1s and 48% higher than GFASv1.2 based on the cloud-adjusted FREM values, and substantially more when the low FRP fire adjustment is included. Fuel consumption rates (Tg biomass.sec^{-1}) for a pixel or grid cell can also be directly estimated from the TPM emission rates via a simple division by the TPM emissions factors (Table 3), providing an estimate of the combustion rate required to produce the inferred TPM fluxes. These fuel consumption rates can be temporally integrated to provide a direct estimate of total fuel consumption if individual gaseous emissions totals are not required. A related approach can be used to derive the equivalent of the FRE-to-dry matter conversion factors (β) of 0.29, 0.78 and 0.96 kg.MJ^{-1} respectively for agriculture, savannah and tropical forest biomes that Kaiser *et al.* (2012) generate via the GFASv1.0 calibration to GFEDv3.1. For low-FRP fire adjusted FREM, we find conversion factors of 1.3 kg.MJ^{-1} for managed lands, 1.1 - 1.6 kg.MJ^{-1} for the various savannah types, and 3.8 kg.MJ^{-1} for closed canopy forest, each derived via satellite observations and TPM EFs alone, rather than calibration against other inventories or independent fuel consumption estimates. These conversion factors are substantially higher than the 0.37 kg.MJ^{-1} found by Wooster *et al.* (2005) during experiments which measured FRE close to laboratory fires, directly because they take into account the factors that affect FRE estimates derived from above the canopy and from Earth orbit discussed in Section 2.

6.3 Extension to Fuel Consumption Per Unit Area

A stated advantage of FREM is that it avoids requiring estimates of fuel consumption per unit area (F_c ; kg.m^{-2}), which typically come from multiplying fuel load and combustion completeness metrics that are generally considered the most uncertain aspects of fire emissions calculations (Reid *et al.,* 2009). However, if F_c is needed FREM can be used to estimate it via the inverse of the Seiler and Crutzen (1980) emissions methodology employed in GFED, i.e. by dividing the grid cell TPM-derived fuel consumption (Section 6.2) by its burned area. Assuming each fire-affected 0.05° grid cell (i.e. those mapped in Fig. 14d) is completely burned, the mapped F_c values for 2011 are shown in Fig. 16a, with magnitudes appearing broadly reasonable compared to the field database of Van Leeuwen *et al*. (2014) and model of Hély *et al.* (2003). Higher *Fc* regions match closely the locations of greater burning reported in Archibald *et al.* (2009), predominantly in the southwest of southern Africa. However, numerous of the grid cells are likely to be only partly burned, so Fig. 16b adjusts for this using the ~ one hundred 500 m spatial resolution MCD64A1 MODIS BA pixels falling in each 0.05° cell. Median F_c values now increase compared to Fig. 16a, to 2.6 (1.8) $kg.m^{-2}$ for Closed Forests, 1.3 (0.9) $kg.m^{-2}$ for Shrublands, 1.1 (0.8) $kg.m^{-2}$ for Managed Lands, 1.9 (1.3) $kg.m^{-2}$ for Open Forests/Woodland Savannah, and 1.0 (0.7) $kg.m^{-2}$ for Grassland Savannah - with (and without) the FREM low FRP fire adjustment applied. Difficulties in mapping small burns with 500 m data (Tsela *et al.,* 2014) mean that some grid cells show zero BA, and so do not report data in Fig. 16b. Closed Forests show a 74% reduction in grid-cell count compared to Fig. 16a, with the other biomes 18 to 47%. Despite lower numbers of reporting cells compared to Fig. 16a, significant spatial variability in F_c is still seen in Fig. 16b, and since MCD64A1 typically underestimates BA (Tsela et al., 2014) F_c values likely tend to overestimation, whereas those of Fig. 16a likely tend to underestimation. Future enhancements to the FREM methodology discussed in Section 7, along with use of new 10 to 30 m spatial resolution BA datasets (e.g. Boschetti *et al.,* 2015) should enable more precise future mapping of F_c via the approach introduced here.

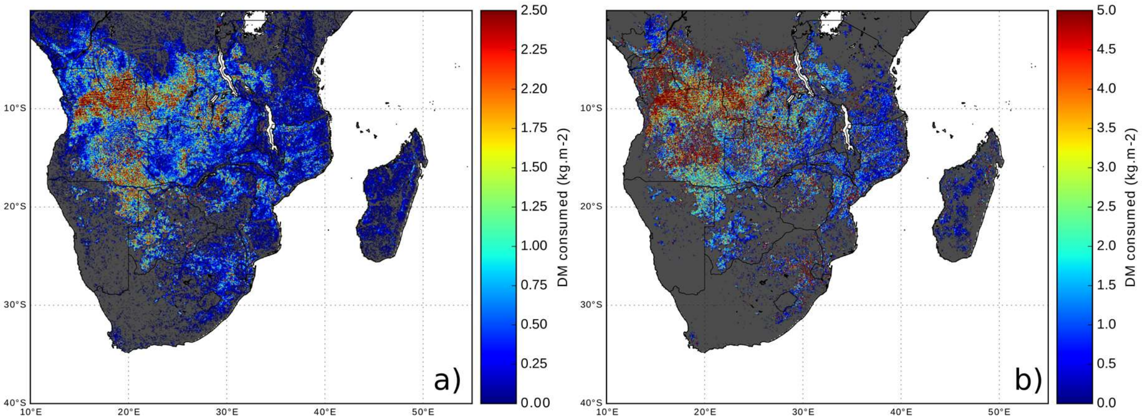

Figure 16. (a) Fuel consumption per unit area (F_c) totals, calculated from the TPM emissions (g.m^{-2}) of Fig. 14d divided by the biome-dependent TPM emissions factor (g.kg^{-1}). (b) These data adjusted for the fraction of the grid cell burned, according to the Collection 6 MCD64A1 MODIS burned area product of Giglio *et al.* (2013). Note colour bar differences between (a) and (b), and that whilst (a) contains data for all grid-cells the SEVIRI FRP-PIXEL Product and the FREM inventory denotes as fire-affected, due to some of these cells reporting zero burned area in the MCD64A1 GFED BA area product there are fewer cells where F_c values can be calculated in (b).

7. CONCLUSIONS

A new 'FRE$_{\text{emissions}}$' (FREM) methodology has been developed to estimate landscape fire emissions of total particulate matter (TPM), trace gases and carbon, based on a combination of geostationary fire radiative energy (FRE) retrievals, polar-orbiting satellite aerosol optical depth (AOD), and particulate and trace gas emissions factors (EFs). 'Smoke emissions coefficients' (which convert FRP into rate of TPM emissions) are derived from matchup FRE and AOD data of a tiny fraction (<< 0.001%) of fires present within the dataset, and these are then applied to the full satellite FRP record to derive TPM emissions, and via use of EF ratios to trace gas and carbon as well. This fully ‘top down’ approach bypasses the fuel consumption step, which is generally considered the most uncertain aspect of fire emissions calculations (Reid *et al.*, 2009; Vermote *et al.*, 2009; van Leeuwen *et al.,* 2014), and thus avoids requiring estimates of fuel load per unit area or combustion completeness. The FREM approach also circumvents use of static, laboratory-derived FRE-to-fuel consumption conversion factors that may not take into account all issues faced when assessing FRE from above the canopy and from Earth orbit (Wooster *et al.*, 2005), whilst also avoiding the need to base such conversion factors on calibrations against bottom-up fuel consumption measures (as is currently done for GFAS; Kaiser *et al.*, 2012), thus providing a totally independent fire emissions estimate to e.g. GFED. If required, fuel consumption per unit area (F_c) measures can be derived a last step to the FREM calculations, based on the inverse of the Seiler and Crutzen (1980) methodology, providing an important new way of mapping this metric across landscapes. Primary uncertainties in FREM pertain to the conversion between AOD and TPM, which relies on the light extinction efficiency per unit of aerosol mass appropriate to biomass burning aerosols (βe, [$m^2.g^{-1}$]), and the degree to which FRE totals need adjusting for undetected low FRP active fire pixels below the geostationary sensors minimum detection limit. These issues will be the subject of future methodological development. Other anticipated improvements relate to use of finer spatial resolution satellite AOD products, and to greater knowledge of the biome and temporal dependency of particulate matter and trace gas emissions factors, required by FREM as they are for all current fire emissions inventories.

Southern African biomass burning emissions fields from 2004-2012 have been generated via the FREM approach applied to Meteosat SEVIRI FRP data available from the EUMETSAT LSA SAF at a far higher spatio-temporal resolution than existing emissions inventories (hourly; 0.05°). Once adjusted for the low-FRP component of a regions fire regime, the monthly TPM, CO_2, CO and

CH_4 totals are similar to those of the MODIS FRP- and AOD-based FEER inventory (Ichoku and Ellison, 2014), though the geostationary FRP-based FREM methodology avoids assumptions regarding plume height and velocity required when using polar-orbiter FRP 'snapshots' (Ichoku and Ellison, 2014). FREM and FEER show significantly higher emissions totals than GFASv1.2 and GFEDv4.1s, with the TPM emissions appearing to align better with estimates provided for southern African biomass burning via remotely sensed AOD (e.g. Tosca *et al.*, 2013) and thus which may agree better with atmospheric studies compared to GFED and GFAS. Whilst the representation of smoke aerosol ageing in atmospheric models will play a part in such comparisons, any confirmed GFED underestimation would stem either from additional undetected or low-biased burned areas, too low fuel consumptions per unit area, or inappropriately low emissions factors. Impacts from each will be transferred to GFAS via its calibration to GFED (Kaiser *et al.*, 2012), but only the latter effect would impact FREM (and then only the trace gas estimates, not those of TPM alone). GFEDv4.1s does report a significant increase in carbon emissions from southern African landscape burning compared to GFEDv3, based on the type of 'small fire boosting' methodology introduced by Randerson *et al.* (2012), suggesting substantial numbers of MODIS AF pixels are located outside of MODIS-mapped burned areas. We also find many areas where the FRP-based FREM reports emissions, but the 500 m MODIS MCD64A1 burned area (BA) product maps zero burning (*c.f.* Fig. 16a and b), but where both provide non-zero data we find calculated fuel consumption per unit area burned (F_c) appear broadly realistic, though with currently large uncertainties at the individual grid-cell level. These will in future be reduced by FREM methodological improvements and higher spatial resolution burned area mapping. Other future work will focus on lessening restrictions on the type of fire available for deriving the smoke emissions coefficients of Fig. 7, as use of the 10 km MODIS AOD product means that large, spatially isolated fires are currently preferred, restricting the number of fires available. The appropriateness of the low-FRP fire adjustment will also be examined, including dependence on view-angle and time of day (Freeborn *et al.*, 2009). The FREM approach will likely benefit from further improvements in the discrimination of fire-relevant biomes, and from enhanced specification of particulate matter emissions factors, something that has generally seen less work than the EFs of trace gases yet which in FREM does impact the trace gas emissions estimates.

FREM provides biomass burning emissions estimates at the highest spatio-temporal scale currently available (i.e. hourly or better, 0.05°), and we believe the technique offers enormous potential to generate datasets suitable for driving detailed plume dispersion modelling that better takes into account fire temporal variability and the strong fire diurnal cycle (e.g. Baldassarre *et al.,* 2015; Roberts *et al.*, 2015). The emissions coefficients necessary to apply the technique to real-time and archived Meteosat SEVIRI FRP-PIXEL data are planned to be made available through the Eumetsat LSA SAF, whilst the fact that Geostationary FRP data are now available from GOES (Xu *et al.*, 2010) and Himawari (Xu *et al.*, 2017) using the same baseline algorithm developed for Meteosat (Wooster *et al.*, 2015; Roberts *et al.,* 2015) means that a consistent, multi-satellite fire emissions dataset for the tropics, sub-tropics and potentially also mid-latitudes is able to be generated using the FREM methodology.

Acknowledgements

MODIS AOD data are distributed freely as part of NASA's MODIS Atmospheric Product Suite (http://ladsweb.nascom.nasa.gov/). SEVIRI FRP-PIXEL data were provided by the EUMETSAT Land Surface Analysis Satellite Application Facility (LSA SAF; https://landsaf.ipma.pt/). We thank the LSA SAF and the developers and providers of the MODIS AOD, GFED and GFAS, as well as Dr Jianging He of King's College London for his support to this effort. Charles Ichoku and Luke Ellison of NASA GSFC provided useful discussions regarding the FEER dataset, and we thank the reviewers for their insightful comments. Funding for this work was provided by EUMETSAT's Satellite Applications Facility Programme (CDOP-2), NERC's National Centre for Earth Observation (NCEO), and the SAMBBA project (NE/J010502/1).

References

Abel, S. J., Haywood, J. M., Highwood, E. J., Li, J., & Buseck, P. R. (2003). Evolution of biomass burning aerosol properties from an agricultural fire in southern Africa. *Geophysical Research Letters*, *30*(15).

Abel, S. J., Highwood, E. J., Haywood, J. M., & Stringer, M. A. (2005). The direct radiative effect of biomass burning aerosols over southern Africa. *Atmospheric Chemistry and Physics*, *5*(7), 1999-2018.

Akagi, S.K., Yokelson, R.J., Wiedinmyer, C., Alvarado, M.J., Reid, J.S., Karl, T., Crounse, J.D. & Wennberg, P.O. (2011). Emission factors for open and domestic biomass burning for use in atmospheric models. *Atmospheric Chemistry and Physics*, *11*(9), pp.4039-4072.

Andela, N., Kaiser, J.W., van der Werf, G.R. and Wooster, M.J. (2015). New fire diurnal cycle characterizations to improve fire radiative energy assessments made from MODIS observations. *Atmospheric Chemistry and Physics*, *15*(15), pp.8831-8846.

Andela, N., van der Werf, G. R., Kaiser, J. W., van Leeuwen, T. T., Wooster, M. J., & Lehmann, C. E. R. (2016) Biomass burning fuel consumption dynamics in the tropics and subtropics assessed from satellite, *Biogeosciences*, *13*, 3717-3734, doi:10.5194/bg-13-3717-2016.

Andreae, M. O., & Merlet, P. (2001). Emission of trace gases and aerosols from biomass burning. *Global biogeochemical cycles*, *15*(4), 955-966.

Andrews, D.P., Lachenbruch, A.H., Mc-Garr, A., Reasenberg, P., Thatcher, W. and Wallace, R.E. (1989). Effects of aerosol from biomass burning on the global radiation budget. *Journal of Geophysical Research*, 94, 12377.

Archibald, S., Roy, D.P., Wilgen, V., Brian, W. & Scholes, R.J. (2009). What limits fire? An examination of drivers of burnt area in Southern Africa. *Global Change Biology*, *15*(3), pp.613-630.

Baldassarre, G., Pozzoli, L., Schmidt, C.C., Unal, A., Kindap, T., Menzel, W.P., Whitburn, S., Coheur, P.F., Kavgaci, A. & Kaiser, J.W. (2015). Using SEVIRI fire observations to drive smoke plumes in the CMAQ air quality model: a case study over Antalya in 2008. *Atmospheric Chemistry and Physics*, *15*(14), pp.8539-8558.

Balsamo, G., Albergel, C., Beljaars, A., Boussetta, S., Brun, E., Cloke, H., Dee, D., Dutra, E., Muñoz-Sabater, J., Pappenberger, F. & De Rosnay, P. (2015). ERA-Interim/Land: a global land surface reanalysis data set. *Hydrology and Earth System Sciences*, *19*(1), pp.389-407.

Bicheron, P., Amberg, V., Bourg, L., Petit, D., Huc, M., Miras, B., Brockmann, C., Hagolle, O., Delwart, S., Ranera, F. & Leroy, M. (2011). Geolocation assessment of MERIS GlobCover orthorectified products. *IEEE Transactions on geoscience and remote sensing*, *49*(8), pp.2972-2982.

Boschetti, L., Eva, H.D., Brivio, P.A. & Grégoire, J.M. (2004). Lessons to be learned from the comparison of three satellite-derived biomass burning products. *Geophysical research letters*, *31*(21).

Boschetti, L., Roy, D.P., Justice, C.O. and Humber, M.L., 2015. MODIS–Landsat fusion for large area 30m burned area mapping. *Remote Sensing of Environment,* 161, pp.27-42.

Van Leeuwen, T.T., Van der Werf, G.R., Hoffmann, A.A., Detmers, R.G., Rücker, G., French, N.H., Archibald, S., Carvalho Jr, J.A., Cook, G.D., De Groot, W.J. and Hély, C., 2014. Biomass burning fuel consumption rates: a field measurement database.

Chin, M., P. Ginoux, S. Kinne, O. Torres, B. N. Holben, B. N. Duncan, R. V. Martin, J. A. Logan, A. Higurashi, and T. Nakajima (2002), Tropospheric aerosol optical thickness from the GOCART Model and comparisons with satellite and Sun photometer measurements, J*ournal of Atmospheric Science*, 59, 461–483.

Chuvieco, E., Giglio, L. and Justice, C. (2008). Global characterization of fire activity: toward defining fire regimes from Earth observation data. *Global Change Biology*, *14*(7), pp.1488-1502.

Delmas, R., Lacaux, J. P., & Brocard, D. (1995). Determination of biomass burning emission factors: Methods and results, *Environ. Monit. Assess., 38*, 181–204, 1995

Edwards, D. (1984). Fire regimes in the biomes of South Africa. In *Ecological effects of fire in South African ecosystems* (pp. 19-37). Springer Berlin Heidelberg.

Ellicott, E., Vermote, E., Giglio, L. & Roberts, G. (2009). Estimating biomass consumed from fire using MODIS FRE. *Geophysical Research Letters*, *36*(13).

Ellison, L. & Ichoku, C. (2015). FEER Coefficient of Emission (Ce) Product User Manual.

Freeborn, P.H., Wooster, M.J., Hao, W.M., Ryan, C.A., Nordgren, B.L., Baker, S.P. & Ichoku, C. (2008). Relationships between energy release, fuel mass loss, and trace gas and aerosol emissions during laboratory biomass fires. *Journal of Geophysical Research: Atmospheres*, *113*(D1).

Freeborn, P.H., Wooster, M.J., Roberts, G., Malamud, B.D. & Xu, W. (2009). Development of a virtual active fire product for Africa through a synthesis of geostationary and polar orbiting satellite data. *Remote Sensing of Environment*, *113*(8), pp.1700-1711.

Freeborn, P.H., Wooster, M.J. & Roberts, G. (2011). Addressing the spatiotemporal sampling design of MODIS to provide estimates of the fire radiative energy emitted from Africa. *Remote Sensing of Environment*, *115*(2), pp.475-489.

Freeborn, P. H., Cochrane, M. A., and Wooster, M. J. (2014) A decade long, multi-scale map comparison of fire regime parameters derived from three publically available satellite-based fire products: a case study in the Central African Republic (2014), *Remote Sensing*, 6, 4061–4089.

Giglio, L., Randerson, J.T., Van der Werf, G.R., Kasibhatla, P.S., Collatz, G.J., Morton, D.C. & DeFries, R.S. (2010). Assessing variability and long-term trends in burned area by merging multiple satellite fire products. *Biogeosciences*, 7(3).

Giglio, L., Randerson, J.T. & Werf, G.R. (2013). Analysis of daily, monthly, and annual burned area using the fourth-generation global fire emissions database (GFED4). *Journal of Geophysical Research: Biogeosciences*, *118*(1), pp.317-328.

Giglio, L., Schroeder, W. & Justice, C.O. (2016). The collection 6 MODIS active fire detection algorithm and fire products. *Remote Sensing of Environment*, *178*, pp.31-41.

Hansen, M.C., DeFries, R.S., Townshend, J.R.G., Sohlberg, R., Dimiceli, C. and Carroll, M., 2002. Towards an operational MODIS continuous field of percent tree cover algorithm: examples using AVHRR and MODIS data. *Remote Sensing of Environment*, 83(1), pp.303-319.

Hély, C., Dowty, P.R., Alleaume, S., Caylor, K.K., Korontzi, S., Swap, R.J., Shugart, H.H. and Justice, C.O., 2003. Regional fuel load for two climatically contrasting years in southern Africa. *Journal of Geophysical Research: Atmospheres*, 108(D13).

Hertwig, D., Burgin, L., Gan, C., Hort, M., Jones, A., Shaw, F., Witham, C. & Zhang, K. (2015). Development and demonstration of a Lagrangian dispersion modeling system for real-time prediction of smoke haze pollution from biomass burning in Southeast Asia. *Journal of Geophysical Research: Atmospheres*, *120*(24), pp.12605-12630.

Hyer, E.J., Kasischke, E.S. & Allen, D.J. (2007). Effects of source temporal resolution on transport simulations of boreal fire emissions. *Journal of Geophysical Research: Atmospheres, 112*(D1).

Huijnen, V., Wooster, M.J., Kaiser, J.W., Gaveau, D.L.A., Flemming, J., Parrington, M., Inness, A., Murdiyarso, D., Main, B. & van Weele, M. (2016). Fire carbon emissions over maritime southeast Asia in 2015 largest since 1997. *Scientific reports*, *6*, p.26886.

Ichoku, C. & Kaufman, Y.J. (2005). A method to derive smoke emission rates from MODIS fire radiative energy measurements. *IEEE transactions on Geoscience and Remote Sensing*, *43*(11), pp.2636-2649.

Ichoku, C., Martins, J.V., Kaufman, Y.J., Wooster, M.J., Freeborn, P.H., Hao, W.M., Baker, S., Ryan, C.A. & Nordgren, B.L. (2008). Laboratory investigation of fire radiative energy and smoke aerosol emissions. *Journal of Geophysical Research: Atmospheres*, *113*(D14).

Ichoku, C. & Ellison, L. (2014). Global top-down smoke-aerosol emissions estimation using satellite fire radiative power measurements. *Atmospheric Chemistry and Physics*, *14*(13), pp.6643-6667.

Intergovernmental Panel on Climate Change (IPCC) (1997). *Revised 1996 IPCC Guidelines for National Greenhouse Gas Inventories Workbook*, 2, 4.23 – 4.28.

Jian, Y. & Fu, T.M. (2014). Injection heights of springtime biomass-burning plumes over peninsular Southeast Asia and their impacts on long-range pollutant transport. *Atmospheric Chemistry and Physics*, *14*(8), pp.3977-3989.

Kaiser, J.W., Heil, A., Andreae, M.O., Benedetti, A., Chubarova, N., Jones, L., Morcrette, J.J., Razinger, M., Schultz, M.G., Suttie, M. & Van Der Werf, G.R. (2012). Biomass burning emissions estimated with a global fire assimilation system based on observed fire radiative power. *Biogeosciences*, *9*(1), pp.527-554.

Keene, W. C., Lobert, J. M., Crutzen, P. J., Maben, J. R., Scharffe, D. H., & Landmann, T. (2006). Emissions of major gaseous and particulate species during experimental burns of southern African biomass, *J. Geophys. Res., 111*, D04301, doi:10.1029/2005JD006319

Knorr, W., Lehsten, V. & Arneth, A. (2012). Determinants and predictability of global wildfire emissions. *Atmospheric Chemistry and Physics*, *12*(15), pp.6845-6861.

Kopacz, M., Jacob, D.J., Fisher, J.A., Logan, J.A., Zhang, L., Megretskaia, I.A., Yantosca, R.M., Singh, K., Henze, D.K., Burrows, J.P. & Buchwitz, M. (2010). Global estimates of CO sources with high resolution by adjoint inversion of multiple satellite datasets (MOPITT, AIRS, SCIAMACHY, TES). *Atmospheric Chemistry and Physics, 10*(3), pp.855-876.

Korontzi, S., Roy, D.P., Justice, C.O. and Ward, D.E., 2004. Modeling and sensitivity analysis of fire emissions in southern Africa during SAFARI 2000. *Remote Sensing of Environment*, 92(2), pp.255-275.

Kukavskaya, E.A., Soja, A.J., Petkov, A.P., Ponomarev, E.I., Ivanova, G.A. & Conard, S.G. (2012). Fire emissions estimates in Siberia: evaluation of uncertainties in area burned, land cover, and fuel consumption. *Canadian Journal of Forest Research*, *43*(5), pp.493-506.

Kremens, R.L., Dickinson, M.B. & Bova, A.S. (2012). Radiant flux density, energy density and fuel consumption in mixed-oak forest surface fires. International Journal of Wildland Fire, 21(6), pp.722-730.

Larkin, N.K., Raffuse, S.M. & Strand, T.M. (2014). Wildland fire emissions, carbon, and climate: US emissions inventories. *Forest Ecology and Management*, *317*, pp.61-69.

Levy, R.C., Mattoo, S., Munchak, L.A., Remer, L.A., Sayer, A.M., Patadia, F. and Hsu, N.C., 2013. The Collection 6 MODIS aerosol products over land and ocean. *Atmos. Meas. Tech*, *6*(11), pp.2989-3034.

Li, Q., Jacob, D. J., Bey, I., Yantosca, R. M., Zhao, Y., Kondo, Y., & Notholt, J. (2000). Atmospheric hydrogen cyanide(HCN): Biomass burning source, ocean sink?. *Geophysical research letters*, *27*(3), 357-360.

Mathews, B.J., Strand, E.K., Smith, A.M., Hudak, A.T., Dickinson, B. & Kremens, R.L. (2016). Laboratory experiments to estimate interception of infrared radiation by tree canopies. *International Journal of Wildland Fire*, *25*(9), pp.1009-1014.

Nogueira, J.M., Ruffault, J., Chuvieco, E. & Mouillot, F. (2016). Can We Go Beyond Burned Area in the Assessment of Global Remote Sensing Products with Fire Patch Metrics?. *Remote Sensing*, *9*(1), p.7.

Paugam, R., Wooster, M., Freitas, S. & Val Martin, M. (2016). A review of approaches to estimate wildfire plume injection height within large-scale atmospheric chemical transport models. *Atmospheric Chemistry and Physics*, *16*(2), pp.907-925.

Pechony, O., Shindell, D.T. & Faluvegi, G. (2013). Direct top-down estimates of biomass burning CO emissions using TES and MOPITT versus bottom-up GFED inventory. *Journal of Geophysical Research: Atmospheres, 118*(14), pp.8054-8066.

Pereira, G., Siqueira, R., Rosário, N. E., Longo, K. L., Freitas, S. R., Cardozo, F. S., Kaiser, J. W., & Wooster, M. J. (2016). Assessment of fire emission inventories during the South American Biomass Burning Analysis (SAMBBA) experiment, *Atmos. Chem. Phys., 16*, 6961-6975, doi:10.5194/acp-16-6961-2016.

Randerson, J.T., Chen, Y., Werf, G.R., Rogers, B.M. & Morton, D.C. (2012). Global burned area and biomass burning emissions from small fires. *Journal of Geophysical Research: Biogeosciences*, *117*(G4).

Reddington, C. L., Spracklen, D. V., Artaxo, P., Ridley, D. A., Rizzo, L. V., & Arana, A. (2016). Analysis of particulate emissions from tropical biomass burning using a global aerosol model and long-term surface observations, *Atmos. Chem. Phys., 16*, 11083-11106, doi:10.5194/acp-16-11083-2016.

Reid, J.S., Koppmann, R., Eck, T.F. & Eleuterio, D.P. (2005). A review of biomass burning emissions part II: intensive physical properties of biomass burning particles. *Atmospheric Chemistry and Physics*, *5*(3), pp.799-825.

Reid, J.S., Hyer, E.J., Prins, E.M., Westphal, D.L., Zhang, J., Wang, J., Christopher, S.A., Curtis, C.A., Schmidt, C.C., Eleuterio, D.P. & Richardson, K.A. (2009). Global monitoring and forecasting of biomass-burning smoke: Description of and lessons from the Fire Locating and Modeling of Burning Emissions (FLAMBE) program. *IEEE Journal of Selected Topics in Applied Earth Observations and Remote Sensing*, *2*(3), pp.144-162.

Roberts, G.J. & Wooster, M.J. (2008). Fire detection and fire characterization over Africa using Meteosat SEVIRI. *IEEE Transactions on Geoscience and Remote Sensing*, *46*(4), pp.1200-1218.

Roberts, G., Wooster, M.J. & Lagoudakis, E. (2009). Annual and diurnal african biomass burning temporal dynamics. *Biogeosciences*, *6*(5).

Roberts, G., Wooster, M.J., Freeborn, P.H. & Xu, W. (2011). Integration of geostationary FRP and polar-orbiter burned area datasets for an enhanced biomass burning inventory. *Remote Sensing of Environment*, 115(8), pp.2047-2061.

Roberts, G., Wooster, M.J., Xu, W., Freeborn, P.H., Morcrette, J.J., Jones, L., Benedetti, A. & Kaiser, J. (2015). LSA SAF Meteosat FRP Products: part 2–evaluation and demonstration of use in the Copernicus Atmosphere Monitoring. *Atmospheric Chemistry and Physics*, *15*(22), pp.13241-13267.

Sayer, A.M., Hsu N.C., Bettenhausen C. & Jeong, M.J. (2013). Validation and uncertainty estimates for MODIS Collection 6 "Deep Blue" Aerosol data. *Journal of Geophysical Research: Atmospheres*, 118, pp.7864-7872.

Sayer, A.M., Munchak, L.A., Hsu, N.C., Levy, R.C., Bettenhausen, C. & Jeong, M.J. (2014). MODIS Collection 6 aerosol products: Comparison between Aqua's Deep Blue, Dark Target, and "merged" data sets, and usage recommendations. *Journal of Geophysical Research: Atmospheres*, *119*(24).

Schroeder, W., Prins, E., Giglio, L., Csiszar, I., Schmidt, C., Morisette, J. & Morton, D. (2008). Validation of GOES and MODIS active fire detection products using ASTER and ETM+ data. *Remote Sensing of Environment*, *112*(5), pp.2711-2726.

Schroeder, W., Oliva, P., Giglio, L. & Csiszar, I.A. (2014). The New VIIRS 375m active fire detection data product: Algorithm description and initial assessment. *Remote Sensing of Environment*, *143*, pp.85-96.

Shi, Y., Matsunaga, T., Saito, M., Yamaguchi, Y. & Chen, X. (2015). Comparison of global inventories of CO 2 emissions from biomass burning during 2002–2011 derived from multiple satellite products. *Environmental Pollution, 206,* pp.479-487.

Seiler, W. and Crutzen, P.J., 1980. Estimates of gross and net fluxes of carbon between the biosphere and the atmosphere from biomass burning. *Climatic change*, 2(3), pp.207-247.

Soares, J., Sofiev, M. & Hakkarainen, J. (2015). Uncertainties of wild-land fires emission in AQMEII phase 2 case study. *Atmospheric* Environment, 115, pp.361-370.

Sofiev, M., Ermakova, T. & Vankevich, R. (2012). Evaluation of the smoke-injection height from wild-land fires using remote-sensing data. *Atmospheric Chemistry and Physics*, *12*(4), pp.1995-2006.

Sommers, W.T., Loehman, R.A. & Hardy, C.C. (2014). Wildland fire emissions, carbon, and climate: science overview and knowledge needs. *Forest Ecology and Management*, *317*, pp.1-8.

Sophie, B., Pierre, D., & Eric, V. B. (2010). *GlobCOVER 2009 products description and validation report.* UCLouvain and ESA.

Tsela, P., Wessels, K., Botai, J., Archibald, S., Swanepoel, D., Steenkamp, K. and Frost, P. (2014). Validation of the two standard MODIS satellite burned-area products and an empirically-derived merged product in South Africa. *Remote Sensing,* 6(2), pp.1275-1293.

Tosca, M. G., Randerson, J. T., & Zender, C. S. (2013). Global impact of smoke aerosols from landscape fires on climate and the Hadley circulation. *Atmospheric Chemistry and Physics*, *13*(10), 5227-5241.

Van der Werf, G. R., Morton, D. C., DeFries, R. S., Olivier, J. G., Kasibhatla, P. S., Jackson, R. B., Collatz, G. J. & Randerson, J. T. (2009). CO_2 emissions from forest loss. *Nature Geoscience*, *2*(11), 737-738.

Van der Werf, G.R., Randerson, J.T., Giglio, L., Collatz, G.J., Mu, M., Kasibhatla, P.S., Morton, D.C., DeFries, R.S., Jin, Y.V. & van Leeuwen, T.T. (2010). Global fire emissions and the contribution of deforestation, savanna, forest, agricultural, and peat fires (1997–2009). *Atmospheric Chemistry and Physics*, *10*(23), pp.11707-11735.

Werf, G.R., Randerson, J.T., Giglio, L., Leeuwen, T.T.V., Chen, Y., Rogers, B.M., Mu, M., van Marle, M.J., Morton, D.C., Collatz, G.J. and Yokelson, R.J. (2017) Global fire emissions estimates during 1997–2016. *Earth System Science Data*, 9(2), pp.697-720.

Van Leeuwen, T.T. & Van Der Werf, G.R. (2011). Spatial and temporal variability in the ratio of trace gases emitted from biomass burning. *Atmospheric Chemistry and Physics*, *11*(8), pp.3611-3629.

van Leeuwen, T. T., van der Werf, G. R., Hoffmann, A. A., Detmers, R. G., Rücker, G., French, N. H. F., Archibald, S., Carvalho Jr., J. A., Cook, G. D., de Groot, W. J., Hély, C., Kasischke, E. S., Kloster, S., McCarty, J. L., Pettinari, M. L., Savadogo, P., Alvarado, E. C., Boschetti, L., Manuri, S., Meyer, C. P., Siegert, F., Trollope, L. A., & Trollope, W. S. W. (2014). Biomass burning fuel consumption rates: a field measurement database, *Biogeosciences, 11*, 7305-7329, doi:10.5194/bg-11-7305-2014.

Vermote, E., Ellicott, E., Dubovik, O., Lapyonok, T., Chin, M., Giglio, L. & Roberts, G.J. (2009). An approach to estimate global biomass burning emissions of organic and black carbon from MODIS fire radiative power. *Journal of Geophysical Research: Atmospheres, 114*(D18).

Weise, D.R. & Wright, C.S. (2014). Wildland fire emissions, carbon and climate: Characterizing wildland fuels. *Forest Ecology and Management*, 317, pp.26-40.

Weinman, J.A. and Olson, W.S. (1981) Infrared radiation emerging from smoke produced by brush fires. *Applied optics*, 20, 199-206.

Wiedinmyer, C., Akagi, S.K., Yokelson, R.J., Emmons, L.K., Al-Saadi, J.A., Orlando, J.J. & Soja, A.J. (2011). The Fire INventory from NCAR (FINN): a high resolution global model to estimate the emissions from open burning. *Geoscientific Model Development*, *4*, p.625.

Wooster, M.J. (2002). Small-scale experimental testing of fire radiative energy for quantifying mass combusted in natural vegetation fires. *Geophysical Research Letters*, 29(21).

Wooster, M.J., Zhukov, B. & Oertel, D. (2003). Fire radiative energy for quantitative study of biomass burning: Derivation from the BIRD experimental satellite and comparison to MODIS fire products. *Remote Sensing of Environment*, *86*(1), pp.83-107.

Wooster, M.J., Roberts, G., Perry, G.L.W. & Kaufman, Y.J. (2005). Retrieval of biomass combustion rates and totals from fire radiative power observations: FRP derivation and calibration relationships between biomass consumption and fire radiative energy release. *Journal of Geophysical Research: Atmospheres*, *110*(D24).

Wooster, M.J., Freeborn, P.H., Archibald, S., Oppenheimer, C., Roberts, G.J., Smith, T.E.L., Govender, N., Burton, M. & Palumbo, I. (2011) Field determination of biomass burning emission ratios and factors via open-path FTIR spectroscopy and fire radiative power assessment: headfire, backfire and residual smoldering combustion in African savannas. *Atmospheric Chemistry and Physics*, *11*(22), pp.11591-11615.

Wooster, M.J., Roberts, G., Freeborn, P.H., Govaerts, Y., Beeby, R., He, J., Lattanzia, A. & Mullen, R. (2015). Meteosat SEVIRI Fire Radiative Power (FRP) products from the Land Surface Analysis Satellite Applications Facility (LSA SAF): Part 1-algorithms, product contents & analysis. *Atmospheric Chemistry and Physics*, *15*(22), pp.13217-13239.

Xu, W., Wooster, M. J., Roberts, G., & Freeborn, P. (2010). New GOES imager algorithms for cloud and active fire detection and fire radiative power assessment across North, South and Central America. *Remote Sensing of Environment*, *114*(9), 1876-1895.

Xu, W., Wooster, M. J., Zhang., T. (2017) Major Advances in Geostationary Fire Radiative Power (FRP) Retrieval over Asia and Australia Stemming from use of Himarawi-8 AHI, *Remote Sensing of Environment,* 193, 138-149.

Zhang, T., Wooster, M.J. and Xu, W. (2017) Approaches for synergistically exploiting VIIRS I- and M-Band data in regional active fire detection and FRP assessment: A demonstration with respect to agricultural residue burning in Eastern China. *Remote Sensing of Environment*, 198, pp.407-424.

LIST OF FIGURE CAPTIONS

Figure 1. Mapped difference (hrs) between the time of maximum active fire pixel count (i.e. daily fire activity peak) and the ± 1 hr window encompassing the MODIS local solar overpass time (which depends on changing location within the MODIS swath). Data are for 2010 and based on Meteosat Second Generation (MSG) SEVIRI FRP-PIXEL Product available from the EUMETSAT LSA SAF (Wooster *et al.*, 2015), spatially aggregated into 0.5° grid cells. Subset graphs show example histograms of FRP-PIXEL active fire detections for three 0.5° grid cells located over eastern Central African Republic, Northern Mozambique, and southern Kenya, with a functional fit to these data and the four MODIS overpass windows per day also indicated. Only fire detections with confidences > 50% are included (Wooster *et al.,* 2015).

Figure 2. Spatial distribution of active fire detection opportunities offered by the MODIS sampling windows shown in Fig. 1. This is expressed as the ratio of the Meteosat SEVIRI FRP-PIXEL active fire detections made within the ± 1 hr window surrounding the four daily MODIS overpass times (shown in Fig. 1) to the total number of daily detections. Source data are those of Fig. 1.

Figure 3. FREM biome map of southern Africa, based on reclassification of the GLOBCOVER 2009 landcover map and appearing similar to the woodland/grassland classification of southern Africa derived by Korontzi *et al.* (2004). Outlines show the thirty-one 500 km × 500 km target regions from which matchup fires used to generate the biome-dependent FREM smoke emissions coefficients (C_{biome}) of Fig. 7 were selected. Red outlined region has its FRP time-series shown in Fig. 4.

Figure 4. Time series of SEVIRI hourly active fire pixel detections (grey bins) and hourly FRE (black line) for the 500 km × 500 km region highlighted in red in Fig.3 in August 2011, located south of the Okavango Delta (see imagery in Fig. 5). Overpass times of Terra and Aqua MODIS are shown by green and blue vertical lines respectively, alongside daily solar noon (red) and the daily time of minimum fire activity minimum (magenta). Error bars on hourly FRE are calculated from the FRP uncertainties delivered in the geostationary FRP-PIXEL product (Wooster *et al.*, 2015).

Figure 5. Example region of southern Africa from which matchup fires were selected on the afternoon of 12th Aug 2011, 12:40 UTC (MODIS Aqua overpass). (a) Region outlined in red in Fig. 3, south of the Okavango delta, depicted as a colour composite using data from the Aqua MODIS afternoon overpass [RGB=1(0.6μm), 4(0.55μm), 3(0.47μm)]. Smoke plumes from candidate active fires are outlined with yellow vectors, and the centre locations of each SEVIRI active fire pixel detected from the time of the identified active fire minimum (shown in Fig. 4) up until this Aqua overpass time are shown as red dots. (b) Zoom around the bottom left fire and

plume shown in (a) to indicate detail. The dark burn scar left by the fire can clearly be seen. (c) Matching MYD04_L2 AOD data derived from the Aqua MODIS overpass shown in (b).

Figure 6. MODIS Aerosol optical depth (AOD) data matching the MODIS image shown in Fig. 5a. The yellow outlines from Fig. 5 here encompass the set of 10 km × 10 km MODIS AOD product pixels that are included in the plume-integrated AOD calculation for each fire. Any pixel partly or wholly encompassed by the vector is included in the AOD summation, which is then used to estimate the mass of total particulate matter in the plume. Some areas of apparently high AOD are unrelated to biomass burning and so are not outlined here, for example that immediately south of the Okavango Delta (*cf.* Fig. 5) neighbouring a highly reflective salt pan.

Figure 7. Biome dependent smoke emissions coefficients (C_{biome}, g.MJ^{-1}) derived from the slope of the linear best fit made between the amount of total particulate matter in a plume (grams) and the amount of radiative energy released by the causal fire (FRE, MJ). Red shaded area represents the 95% confidence interval on this slope (i.e. the uncertainty in C_{biome}), whilst the grey shaded area represents the prediction interval (i.e. the interval encompassing to 95% probability the value of TPM given a single value of FRE). Coefficients are shown for the biomes of (a) Closed Canopy Forest, (b) Open Canopy Forest and Woodland (Woodland Savanna), (c) Shrublands, (d) Grasslands (Grassland Savanna), and (e) Managed lands (including Croplands). For each biome, each data point represents a single fires FRE calculated from a series of Meteosat FRP-PIXEL products (Fig. 4), and specifically from the fire activity minimum up until the time of the satellite overpass from which the matching smoke plume TPM was estimated from the MODIS AOD

product (Fig. 5; Fig. 6). Uncertainties in FRE (1σ) are derived from the FRP-PIXEL uncertainty metrics (Wooster *et al.*, 2015), whereas those in TPM are derived from the ±1.0 $m^2.g^{-1}$ uncertainty in the assumed smoke aerosol extinction cross-section (Table 1) and the MODIS AOD uncertainty layer. MODIS AOD uncertainties estimates correspond to one-standard-deviation Gaussian confidence interval of the envelopes resulting from the comparison of retrieved AOD data and AERONET measures. These depend on the AOD, QA flag, and viewing geometry (Sayer *et al.,* 2013).

Figure 8. Monthly total particulate emissions estimates for southern African fires, derived from the $FRE_{emissions}$ methodology (FREM) applied to the SEVIRI FRP-PIXEL product of Wooster *et al.* (2015) for 2004-2012. Three versions are shown, those based on 'raw' SEVIRI FRP observations, those adjusted for cloud cover, and those adjusted for 'cloud cover and under-detected low FRP fires' (see Section 5.1 and 5.2). The associated uncertainties are shown in each case. Corresponding TPM emissions from the GFED v4.1s, GFAS v1.2 and FEER v1.0 inventories are shown for comparison, and the cloud and low FRP fire adjusted FREM values calculated from SEVIRI lie very close to the MODIS-derived FEER estimates.

Figure 9. Percentage of daily FRE calculated from the Meteosat SEVIRI FRP-PIXEL product for 2012 that is released (a) during the ± 1 hr window encompassing the MODIS overpass time, and (b) in each biome. For comparison to the percentage values, fire activity expressed as daily FRE from MSG SEVIRI is also shown (grey line, scaled from 0 to 100%).

Figure 10. Cumulative sum of FREM-derived TPM emissions (%), expressed as function of the per-grid cell FREM-to-GFED v4.1s emissions ratio. Calculations were performed using the 0.25° grid cells of GFED, and 85% of cells had non-zero values in both inventories. < 1% of cells had a non-zero Colours are the same as those mapped in Fig. 3. (a) shows the results using the cloud-corrected FREM, and (b) the cloud and low FRP fire corrected FREM.

Figure 11. Emission rates of total particulate matter (TPM) coming from landscape fires in 2012 across southern Africa, as derived from the FREM methodology applied to SEVIRI FRP-PIXEL data, and from GFEDv4.1s, GFASv1.2 and FEERv1.1. GFAS and FEER provide daily values, and GFED monthly values. All are shown as equivalent daily mean rates for comparison, but the FREM-derived values can be calculated at up to 15-min temporal resolution direct from the SEVIRI FRP observations. In addition to FREM daily means, FREM-hourly averages are therefore also shown (rhs y-axis), and these show far higher daytime peaks than the daily averages.

Figure 12. Data of Fig. 11 shown only for August 2012 to see more detail, particularly of the strong diurnal variability in TPM emissions enabled by the FREM approach.

Figure 13. Total particulate matter (TPM) emission density (g.m^{-2} equivalent averaged over each grid cell) for the 25,000 km^{2} area of southern Africa outlined in red in Fig. 3 for 2011, as depicted by (a) GFEDv4.1s (0.25° grid cells), (b) GFASv1.2 (0.1° grid cells), (c) FEERv1.1 (0.1° grid cells)

and (d) FREM inventory (0.05 ° grid cells). The coarser the grid resolution typically the lower the emission density values, since many of the fires typically do not cover entire cells, particularly for the coarser-scale inventories. Results for the FREM cloud and small fire adjusted inventory are shown in (d), with a different colour-bar than for the other inventories. Values for the cloud-adjusted FREM inventory can simply be provided by using the colour bar shown in (a), (b) and (c) also for (d).

Figure 14. Total particulate matter (TPM) emission density (g.m^2) across all of southern Africa in 2011, as depicted by (a) GFEDv4.1s (0.25 ° resolution), GFASv1.2 (0.1 ° resolution), FEERv1.1 (0.1 ° resolution) and the SEVIRI FRP-derived FREM inventory (0.05 ° resolution). See Fig. 13 and its caption for more detail, and note the differing colour bar of (d).

Figure 15. Monthly emissions (Tg) of CO_2, CO and CH_4 for southern Africa (2004-2012) for the FREM inventory, along with those of GFEDv4.1s, GFASv1.2 and FEERv1.1.

Figure 16. (a) Fuel consumption per unit area (F_c) totals, calculated from the TPM emissions (g.m^{-2}) of Fig. 14d divided by the biome-dependent TPM emissions factor (g.kg^{-1}). (b) These data adjusted for the fraction of the grid cell burned, according to the Collection 6 MCD64A1 MODIS burned area product of Giglio *et al.* (2013). Note colour bar differences between (a) and (b), and that whilst (a) contains data for all grid-cells the SEVIRI FRP-PIXEL Product and the FREM inventory denotes as fire-affected, due to some of these cells reporting zero burned area in the MCD64A1 GFED BA area product there are fewer cells where F_c values can be calculated in (b).